Czech Technical University in Prague
Faculty of Nuclear Sciences and Physical Engineering

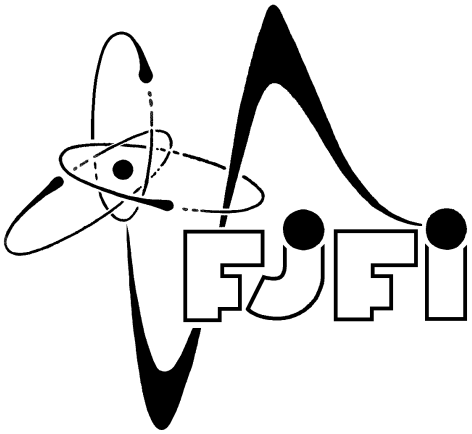

Diploma Thesis

Czech Technical University in Prague
Faculty of Nuclear Sciences and Physical Engineering

Diploma Thesis

Physics with High pT Jets at DØ

Zdeněk Hubáček

Department of Physics
Academical Year: 2003/2004
Supervisor: Vladislav Šimák

Prohlašuji, že jsem svou diplomovou práci vypracoval samostatně a použil jsem pouze podklady (literaturu, projekty, SW atd.) uvedené v přiloženém seznamu.

Nemám závažný důvod proti užití tohoto školního díla ve smyslu § 60 Zákona č. 121/2000 Sb., o právu autorském, o právech souvisejících s právem autorským a o změně některých zákonů (autorský zákon).

I declare that I have written this diploma thesis independently using the listed references. I agree with using this diploma thesis.

Zdeněk Hubáček

Acknowledgement

I would like to thank very much my supervisor Vladislav Šimák for his leadership during last three years and for giving me the possibility to join the DØ experiment at Fermilab.

For the diploma thesis I appreciate very much the help and advice from Alexander Kupčo and Jiří Kvita.

Contents

List of Figures

List of Tables

1 Introduction

Elementary particle physics is searching for the building blocks of matter. This search is currently done on large machines called accelerators, where scientists examine data coming from huge detectors. As they improve their knowledge, the search is getting tougher and tougher. To find new phenomena larger effort has to be made.

Current largest particle accelerator, Tevatron, is situated at the Fermi National Accelerator Laboratory near Chicago, USA. At the Tevatron two major experiments are conducted - CDF and DØ. Their biggest discovery was the observation of the top quark in 1995. The Tevatron underwent a major upgrade and has started a new period of data taking in 2001 (Run II).

The top quark perfectly fits in the Standard Model theory. However in this theory one particle is missing. The Higgs boson still awaits its discovery. The CDF and DØ experiments are trying as much as possible to find it, while it also searches for new phenomena beyond the Standard Model.

This thesis performs an analysis of the data collected in the DØ experiment in Run II from August 2002 to September 2003. It studies properties of the inclusive dijet production and associated lepton production. The dijet studies serve for comparison with the theory of strong interaction called Quantum Chromodynamics. The associated lepton production is usually helpful in investigating particle properties.

The thesis starts with a brief review of the current knowledge about elementary particles and leads to the definition of a jet from an experimental point of view. Then it explains properties of jet algorithms and describes their two main classes. Next section covers a brief description of the accelerator complex and the DØ experiment. The Data Analysis section describes how the analysis was performed and shows its results.

2 High-energy Physics

2.1 Historical Overview

Physics belongs to natural sciences. Its main goal is to try to answer the ultimate questions about the universe. While leaving the question 'Why?' to philosophy, it at least tries to answer 'How?'.

Particle (or High-energy) physics is looking for the smallest constituents of matter and for the tools, how to describe their behavior. Today, physicist's concept of the universe's building blocks is the Standard Model. But due to a large number of parameters it is probably not the final theory.

Standard Model is about thirty years old, but the search for the smallest components of matter has interested people for much longer time. The first one usually mentioned is a Greek philosopher Democritos, who looked at things around him as built of small parts, which he called $\acute{\alpha}\tau o\mu o$ (indivisible in Greek).

Skipping more than two thousand years, the next major step was done in chemistry. Investigating properties of chemical reactions John Dalton was able to conclude that the reactions are due to combining of basic constituents, which were therefore called atoms. At that time, this experimentally confirmed the Democritos's idea, but some two hundred years later things changed again. At the end of 19th century, while experimenting with cathode rays, J.J. Thomson discovered something which looked like a particle, but its mass was nearly two thousand times smaller than the mass of the lightest chemical atom. To be more confused, it looked like that this particle (called electron now) appeared to come from atoms, so the concept of indivisible atoms was lost.

While examining the structure of an atom (an electron carries an electric charge, while atom is electrically neutral), E. Rutherford was able to show, that inside an atom there is a small center carrying a positive charge - an atomic nucleus.

Later other surprising things were discovered - positron (a positively charged partner of electron) in 1932 by C. Anderson (fitting into a theory developed few years sooner), proton and neutron.

Within next two decades a lot of new particles were discovered and that was a signal that we need a new theory to organize these particles

On the other hand, theoretical concepts describing particle physics involve both major theories discovered in the last century - theory of relativity and quantum mechanics.

2.2 Standard Model

Our current knowledge about elementary particles is described by the Standard Model. According to the Standard Model, all matter is formed by quarks and leptons that interact among themselves. These interactions have an exchangeable character; all interacting particles exchange other particles among themselves.

To summarize the Standard Model, it consists of 3 generations of quarks (each generation containing 2 quarks), 3 generations of leptons (to each lepton one associated neutrino), to all these particles their antiparticles, and particles of interactions (a photon for electromagnetic, gluons for strong and $W^{\pm}, Z^0$ bosons for weak interaction). Gravitational force is not considered on the level of particles. The last particle is the Higgs boson responsible for particle masses.

Standard Model has been a very successful theory. All the foretold particles were discovered (excluding the Higgs). Also being about 30 years old, it is still consistent with recent data. On the other hand, we are sure, that it is not a final theory. Standard Model depends on about 20 parameters which must be added by hand (masses of particles and coupling constants).

There are many extensions beyond the Standard Model (including SUSY), or theories describing force unifications (super-strings, GUT). For confirming

or disproving them we do not however have available machine. We hope that future results from the Tevatron and from the LHC will solve these questions.

	1^{st} generation	2^{nd} generation	3^{rd} generation
Quarks	u (up)	c (charm)	t (top)
	d (down)	s (strange)	b (bottom)
Leptons	e^- (electron)	μ^- (muon)	τ^- (tau lepton)
Neutrinos	ν_e	ν_μ	ν_τ
	Forces		
Force Carriers	Electrodynamic	Weak	Strong
	γ (photon)	$W^\pm, Z^0$	g (gluons)
Higgs boson	H		

Table 2.1: Table of Elementary Particles

Standard Model is a $SU(3) \times SU(2) \times U(1)$ gauge field theory. That means that all the particles are described as fields in the Lagrangian. The gauge invariance gives rise to the force carriers ($SU(3)$ gauge invariance leads to the existence of gluons, $SU(2)$ and $U(1)$ to weak vector bosons and photon). While the gluons and the photon are massless, the vector bosons do have a mass. They acquire their mass via the Higgs mechanism and the spontaneous symmetry breaking. The Higgs mechanism can also in a similar way assign the mass to quarks and leptons.

From the Lagrangian one can get the equations of motion. Unfortunately these equations are too complicated, so one cannot solve them directly. Instead we can only use an approximation method of the perturbative theory.

On the quantum level, where the particles (fields) are described in terms of creation and annihilation operators, the perturbation theory can be described with the help of Feynman diagrams. The incoming and outgoing particles are drawn as incoming and outgoing lines. Their interaction is drawn as a vertex and the exchanged particles are drawn as internal lines, called propagators. When these diagrams are assigned with the Feynman

rules, the matrix element of the process can be easily calculated. From the matrix element one can easily get the cross-section or other desired quantity.

The strong force is described by the Quantum Chromodynamics (QCD). QCD is a $SU(3)$ gauge theory. $SU(3)$ is non-Abelian Lie Group with $3^2-1 = 8$ generators. This means that the interaction of quarks is mediated by other particles called gluons. The non-Abelian property of the group gives birth to interaction between gluons, so the spectrum of possible interactions is much richer compared to Abelian case in Quantum Electrodynamic, where photons can not interact directly among themselves.

QCD Lagrangian can be written as

$$L = -\frac{1}{4}F^a_{\mu\nu}F^{a\mu\nu} + \sum_i \overline{\psi}_i(\not{D} - m_i)\psi_i. \tag{2.1}$$

The first part is the kinetic term of the gluon field. The field strength tensor is

$$F^a_{\mu\nu} = \partial_\mu A^a_\nu - \partial_\nu A^a_\mu + g f^{abc} A^b_\mu A^c_\nu, \tag{2.2}$$

where the last term must be there to maintain the gauge invariance. This term is also responsible for self-gluon interaction. While quarks are fermions, their term in the Lagrangian is a density of a Dirac field. QCD introduces a new charge called color, so the basic mathematical quantity describing a quark is the matrix in the color space

$$\psi(x) \equiv \begin{pmatrix} \psi^1(x) \\ \psi^2(x) \\ \psi^3(x) \end{pmatrix}. \tag{2.3}$$

$$D_\mu = \partial_\mu - igA^a_\mu T^a, \tag{2.4}$$

is the covariant derivative, T^a are the generators of the SU(3) group and $\not{D} = \gamma^\mu D_\mu$.

Two kinds of infinities appear in perturbative QCD (pQCD) calculations. The first one is associated with the divergence in the integration over large values of momenta in the loop diagrams (UV divergence), the second one is connected with the integration over small values of loop momenta (is therefore called IR divergence) or whenever two partons in the final state are collinear or one of the final state partons is soft).

The UV divergences are dealt with renormalization procedure. The divergences are absorbed by redefinition of the coupling constant, masses and wave functions. This renormalizability is an important feature of QCD. The renormalization procedure introduces a scale μ on which the redefined parameters depend. The observables should be independent of this scale, but the truncation of perturbative series at some fixed order violates this independence. For example in the common renormalization scheme called $\overline{\text{MS}}$ scheme (modified minimal subtraction) the dependence of the strong coupling constant on the scale μ is given by

$$\mu \frac{\mathrm{d}\alpha_S(\mu/\Lambda)}{\mathrm{d}\mu} = \beta(\alpha_S(\mu/\Lambda)). \tag{2.5}$$

Since the scale has a dimension of energy and coupling constant is dimensionless, additional parameter Λ with a dimension of energy must be introduced. Expanding the β function in a series,

$$\beta(\alpha_S) = -\beta_0 \frac{\alpha_S^2}{2\pi} - \beta_1 \frac{\alpha_S^3}{(2\pi)^2} - \cdots, \tag{2.6}$$

the first coefficients are:

$$\beta_0 = 11N_c - \frac{2}{3}n_f, \qquad \beta_1 = \frac{1}{3}(51N_c - 19n_f), \tag{2.7}$$

with N_c the number of colors and n_f number of quark flavors in theory ($N_c = 3$ and $n_f = 6$ for the Standard Model). At the leading order (i.e. taking into account only the β_0 term) the eq. (2.6) can be solved easily obtaining

$$\alpha_S(\mu/\Lambda) = \frac{1}{\frac{\beta_0}{2\pi}\ln(\mu/\Lambda)}. \tag{2.8}$$

One can see that α_S decreases with increasing μ and approaches zero when μ goes to infinity. This type of behavior is the so-called asymptotic freedom. This feature of the QCD allows us to treat the partons (quarks and gluons) inside proton as free particles in high energy limit. The parameter Λ determines the region, where the perturbative theory is not adequate (Λ is of the order of a few hundreds MeV).

The treatment of IR divergences is different. Instead of redefining quantities, they are canceled if all physically indistinguishable initial and final states are properly taken into account in the definition of observables.

A summary of matrix elements for the simplest two-body processes in QCD are listed in table 2.2. The normalization is such that

$$\frac{\mathrm{d}\sigma}{\mathrm{d}t} = \frac{1}{16\pi s^2}\langle|M|^2\rangle \tag{2.9}$$

and in the CMS

$$t = -2E^{\star 2}(1-\cos\theta^\star). \tag{2.10}$$

Process	$\langle\|M\|^2\rangle/g^4$
$q_\alpha q_\beta \to q_\alpha q_\beta$	$\frac{2}{9}\left[\frac{2\left(s^2+u^2\right)}{t^2} + \left(\frac{2\left(t^2+s^2\right)}{u^2} - \frac{1}{3}\frac{4s^2}{ut}\right)\delta_{\alpha\beta}\right]$
$q_\alpha \overline{q}_\beta \to q_\alpha \overline{q}_\beta$	$\frac{2}{9}\left[\frac{2\left(s^2+u^2\right)}{t^2} + \left(\frac{2\left(t^2+u^2\right)}{s^2} - \frac{1}{3}\frac{4u^2}{st}\right)\delta_{\alpha\beta}\right]$
$qg \to qg$	$\left[\left(1-\frac{us}{t^2}\right) - \frac{4}{9}\left(\frac{s}{u}+\frac{u}{s}\right) - 1\right]$
$gg \to q\overline{q}$	$\frac{1}{6}\left(\frac{u}{t}+\frac{t}{u}\right) - \frac{3}{4}\left(1-\frac{ut}{s^2}\right) + \frac{3}{8}$
$q\overline{q} \to gg$	$\frac{64}{9}\langle\|M_{gg\to q\overline{q}}\|^2\rangle/g^4$
$gg \to gg$	$\frac{8}{9}\left[-\frac{33}{4} - 4\left(\frac{ut}{s^2}+\frac{us}{t^2}+\frac{st}{u^2}\right)\right] - \frac{9}{16}\left[45 - \left(\frac{s^2}{ut}+\frac{t^2}{ut}+\frac{u^2}{ts}\right)\right]$

Table 2.2: List of QCD LO spin and color averaged invariant amplitudes

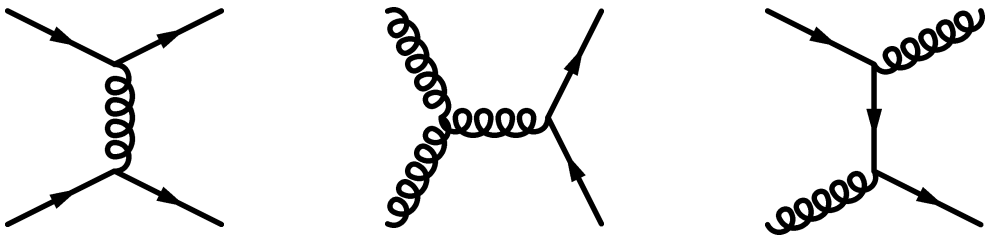

Figure 2.1: LO processes dominant at the Tevatron

2.3 Proton Structure

Since 1964, the proton is no longer considered as an elementary particle. The first model proposed by Gell-Man and Zweig states that protons are formed by three smaller constituents called quarks.

Other model was proposed also in the 1960s to describe the SLAC results of electron-proton scattering. The interesting result of a higher-than-expected number of electron scattered at large angles was interpreted by Feynman and Bjorken as a scattering of electrons on point-like objects inside proton. These point-like objects were called partons.

In 1970s, these two models were united under the QCD described in previous section. The proton contains quarks and gluons, all interacting among themselves. This section will describe how does the proton look like.

In deep inelastic electron-proton scattering the following variables are usually used:

$$Q^2 = -(k - k')^2, \qquad x = \frac{Q^2}{2P \cdot q}, \tag{2.11}$$

with Q^2 representing the negative of the square of the interchanged momentum between the electron and the parton, while x is interpreted as the fraction of the proton momentum carried by the interacting parton. Then the differential cross-section of the process can be written as

$$\frac{\mathrm{d}^2\sigma}{\mathrm{d}x\mathrm{d}Q^2} = \frac{2\pi\alpha^2(1+(1-y)^2)}{xQ^4}\left\{F_2(x,Q^2) - \frac{y^2}{1+(1-y)^2}F_L(x,Q^2)\right\}, \tag{2.12}$$

where y is coefficient of inelasticity and F_2 and F_L are the so-called proton structure function; that means they in some way describe the inner structure of the proton. For $y \leq 0.6$ the dominant part is the one of F_2.

According to experimental results, the partons showed up as spin $\frac{1}{2}$ objects, that means fermions. It looked reasonably if they could be identified as quarks. In this model the structure function can be written as

$$F_2(x,Q^2) = \sum_q e_q^2 x f_q(x,Q^2), \tag{2.13}$$

with $f_q(x, Q^2)$ being the parton distribution (or density) functions characterizing the distribution of quarks (the probability of finding a certain quark flavor carrying a fraction x of the proton momentum in process at some energy scale of Q^2).

To complete the gauge field model with gluons, it is needed to add the comment, that the total momentum carried by quarks in less than $\frac{1}{2}$ of the total momentum of proton. The bigger half therefore belongs to gluons.

2.3.1 Parameterization of Structure Functions

The parton distribution functions (pdfs) are not described by pQCD. The goal of parameterization is to describe their shape as much accurate with respect to experimental data as possible. The pdfs are smooth functions of the two variables x and Q^2 (the fraction of (longitudinal) momentum of proton carried by the interacting parton and the energy scale of the process). In the simplest additive quark model, the x dependence would be $x = \frac{1}{3}$ for all three quarks. This simple approximation is then unsmeared by the QCD interactions among quarks and gluons. However this unsmearing is not described by the QCD and the pdfs dependence is then given only by simple parameterization at some given scale Q_0^2:

$$f_i(x, Q_0^2) = A_0 x^{A_1} (1 - x)^{A_2} P(x; A_3, \ldots). \tag{2.14}$$

The function $P(x; A_3, \ldots)$ can be arbitrary smooth function of one or more parameters A_i.

At least the Q^2 dependence of pdfs is given by QCD. This is described by the DGLAP (or evolution) equations. The equations can be summarized as follows,

$$\frac{\mathrm{d}q_i(x, Q^2)}{\mathrm{d}\ln Q^2} = \frac{\alpha_S(Q^2)}{\pi} \int_x^1 \frac{\mathrm{d}y}{y} \left[P_{qq}^{(0)}\left(\frac{x}{y}\right) q_i(y, Q^2) + P_{qG}^{(0)}\left(\frac{x}{y}\right) G(y, Q^2) \right], \tag{2.15}$$

$$\frac{\mathrm{d}\overline{q}_i(x, Q^2)}{\mathrm{d}\ln Q^2} = \frac{\alpha_S(Q^2)}{\pi} \int_x^1 \frac{\mathrm{d}y}{y} \left[P_{qq}^{(0)}\left(\frac{x}{y}\right) \overline{q}_i(y, Q^2) + P_{qG}^{(0)}\left(\frac{x}{y}\right) G(y, Q^2) \right], \tag{2.16}$$

$$\frac{\mathrm{d}G(x,Q^2)}{\mathrm{d}\ln Q^2} = \frac{\alpha_S(Q^2)}{\pi}\int_x^1 \frac{\mathrm{d}y}{y}\left[P_{Gq}^{(0)}\left(\frac{x}{y}\right)\Sigma(y,Q^2) + P_{GG}^{(0)}\left(\frac{x}{y}\right)G(y,Q^2)\right], \tag{2.17}$$

with

$$\Sigma(x,Q^2) = \sum_{i=1}^{n_f}(q_i(x,Q^2) + \overline{q}_i(x,Q^2)), \tag{2.18}$$

and

$$P_{qq}^{(0)}(x) = P_{\overline{q}\overline{q}}^{(0)}(x) = \frac{4}{3}\left[\frac{1+x^2}{1-x}\right]_+, \tag{2.19}$$

$$P_{qG}^{(0)}(x) = P_{\overline{q}G}^{(0)}(x) = \frac{x^2+(1-x)^2}{2}, \tag{2.20}$$

$$P_{Gq}^{(0)}(x) = P_{G\overline{q}}^{(0)}(x) = \frac{4}{3}\frac{1+(1-x)^2}{x}, \tag{2.21}$$

$$P_{GG}^{(0)}(x) = 6\left\{\left[\frac{x}{1-x}\right]_+ + \frac{1-x}{x} + x(1-x) + \left(\frac{33-2n_f}{36} - 1\right)\delta(x-1)\right\}. \tag{2.22}$$

The splitting functions $P_{ij}^{(0)}(x)$ represent the probabilities for splitting parton i to parton j and something else, the exponent means that these are the LO approximations. The "+" sign is defined as

$$[f(x)]_+ = \lim_{\beta\to 0^+}\left(f(x)\theta\left(1-x-\beta\right) - \delta(1-x-\beta)\int_0^{1-\beta} f(y)\mathrm{d}y\right). \tag{2.23}$$

2.4 Jets

Jets are typical products of high-energy collisions. During these collisions a large number of particles is created. Typical property of these particles is their angular distribution. In most cases all particles fly away from interaction in small number of different ways. From experimentalist point of view, the jets are given by the geometrical arrangement of the energy flow caused by particles going through the detector.

The reduction of a large number of particles to a small number of jets enables us to compare the experimental results with theoretical predictions. As mentioned earlier, according to QCD, the proton is a system of partons (quarks and gluons). In high-energy collisions (protons with antiprotons in Tevatron) only one parton from proton interacts with one parton from

antiproton. This interaction is described by Feynman diagrams and can be calculated with the tools of QCD. Due to factorization theorem, the cross section of some process can be written as

$$\sigma(p\overline{p} \to X) = \sum_{i,j=q,g} \int_0^1 \mathrm{d}x_1 \mathrm{d}x_2 f_i(x_1, \mu) f_j(x_2, \mu) \sigma(ij \to X), \tag{2.24}$$

with X being the chosen final state and μ the energy scale of the process. This means, that the cross-section can be computed if the cross-section on parton level and the parton distributions are known.

After the interaction the partons are flying away. The QCD confinement says that only colorless object can be observed. The process in which partons form colorless hadrons is called hadronization. This process is not understood yet. Only approximate models of it exist. The important comment is, that particle physicists believe, that hadronization is a soft process, that means that it does not change dramatically the energy and angular distribution of outgoing particles, so the correspondence between parton and hadron level is still maintained.

After the hadronization one gets some number of particles in final state. To reduce this number and to form the jets some kind of jet algorithm has to be applied.

The properties of jet algorithms will be summarized in following sections.

2.4.1 Ideal Algorithm

To define a jet algorithm one can start with a list of general properties that should be fulfilled by every jet algorithm:

1. Complete definition: The whole process, all jet variables and the various corrections should be clearly and completely defined. If needed, all other algorithms such as preclustering, merging and splitting have to be described.

2. Good behavior: The algorithm should be infrared and collinear safe without introducing any new unnecessary parameters.

3. Experiment independence: The algorithm should not depend on the detector type and its geometrical properties.

4. Universality: The behavior of the algorithm should be the same at the parton, particle, and detector levels.

2.4.2 Theoretical Properties

From theoretical point of view, the theoretical attributes of the algorithm should be enhanced in the following way:

1. Infrared divergences: They should not appear in the perturbative calculations. The algorithms also should be insensitive to soft radiation. As will be shown later, the class of algorithms with initial seeds do not satisfy this condition.

2. Collinear partons: Again, the collinear singularities should not appear in the perturbative calculations and also the jets should be insensitive to any collinear radiation in the event.

3. Invariance under boosts: For the $p\bar{p}$ interaction the parton-parton center of mass system is usually boosted along the beam axis with the respect to the $p\bar{p}$ center of mass system, the algorithm should then find the same solution independent of boosts. These condition can be modified to other collision different from $p\bar{p}$ stating that appropriate variables should be used (such as holding invariance properties of the studied system).

2.4.3 Experimental Properties

The image of an ideal algorithm is destroyed when the jets enter the detector (or in other words - the real world). Limited detector properties affect the performance of every ideal algorithm. The goal of experimental groups is to correct these effects. Ideally these corrections should not be too large. So additional conditions on the algorithm can be added:

1. Detector independence: The algorithm and its performance should be independent as possible of the detector parameters and properties.

2. Stability with luminosity: Jets should not greatly depend on luminosity. That means that the energy and angular resolution should be independent and also the algorithm should not be strongly affected by multiple hard scattering at high luminosities.

3. Efficiency: The algorithms should be as efficient as possible (reconstructing all physical interesting jets) while at the same time it should minimize the use of computer time and memory.

4. Full specification: All aspects of the algorithm have to be fully specified.

5. Ease of use: The algorithm should be straightforward to implement with typical experimental detectors and data.

2.5 Examples of Jet Algorithms

In this chapter, two main classes of jet algorithms will be described showing their advantages and disadvantages. Generally a jet algorithm consists of four parts. In the beginning, we need to know what type of objects enter the algorithm. Second step determines under which condition is the jet formed. Third step assigns the jet its kinematical properties. At last, additional conditions can be applied to the final state jets.

2.5.1 Cone Algorithm

Cone algorithm has been used in high-energy interaction for a longer time. Therefore there exist a variety of modifications. Basically Cone algorithm merges together particles lying within a cone with its vertex at the interaction point. If the event is described in terms of angular variables η, ϕ, where pseudorapidity *eta* is defined as $\eta = -\ln(\tan\frac{\theta}{2})$ and ϕ is the azimuthal angle. Pseudorapidity is used instead of the polar angle θ because of its transformation properties under boosts in beam axis. Particles form a jet if

they all lie in a circle of radius R

$$(\eta - \eta_{jet})^2 + (\phi - \phi_{jet})^2 \leq R^2. \tag{2.25}$$

Common arrangement is as follows: particles are identified with massless fourvectors ($E^i = |\mathbf{p}^i|, \mathbf{p}^i$) and angles ($\phi^i, \theta^i, \eta^i = -\ln(\tan(\theta^i/2))$) assigned from interaction vertex by a unit vector $\mathbf{p}^i/E^i$. For each particle a scalar variable called transverse energy is computed as $E_T^i = E^i \sin(\theta^i)$. For a possible cone axis (a point in $\eta \times \phi$ plane) all particles that might be in this cone are determined according to (i-th particle belongs to cone jet with axis C if)

$$\sqrt{(\eta^i - \eta^C)^2 + (\phi^i - \phi^C)^2} \leq R. \tag{2.26}$$

For all particles in jet a new axis (N) is computed (E_T weighted sum):

$$\eta^N = \frac{\sum_i E_T^i \eta^i}{E_T^{\rm tot}}, \qquad \phi^N = \frac{\sum_i E_T^i \phi^i}{E_T^{\rm tot}}, \tag{2.27}$$

summing over all particles in jet, $E_T^{\rm tot} = \sum_i E_T^i$.

If the new axis is equal to the initial one $N = C$, it is an stable example and all these particles are assigned to the jet. If the axis are not equal, a new axis is searched for. The algorithm is iterated taking N as a jet axis.

According to this scheme the jet variables are assigned in the following way:

$$E_T^{\rm jet} = \sum_i E_T^i, \tag{2.28}$$

$$\eta^{\rm jet} = \frac{1}{E_T^{\rm jet}} \sum_i E_T^i \eta^i, \tag{2.29}$$

$$\phi^{\rm jet} = \frac{1}{E_T^{\rm jet}} \sum_i E_T^i \phi^i, \tag{2.30}$$

Another scheme recommended for Run II of Tevatron is different in using rapidity $y = \frac{1}{2} \ln \frac{E+p_z}{E-p_z}$ (which for massless particles is equal to pseudorapidity η). Then the particle belongs to a jet, if

$$\sqrt{(y^i - y^C)^2 + (\phi^i - \phi^C)^2} \leq R. \tag{2.31}$$

For the new axis:

$$p^N = (E^N, \mathbf{p}^N) = \sum_i (E^i, p_x^i, p_y^i, p_z^i), \tag{2.32}$$

$$y^N = \frac{1}{2} \ln \frac{E^N + p_z^N}{E^N - p_z^N}, \qquad \phi^N = \tan^{-1} \frac{p_y^N}{p_x^N}. \tag{2.33}$$

Jet is then stable if $y^N = y^C$ and $\phi^N = \phi^C$ and the jet variables are

$$p^{\text{jet}} = (E^{\text{jet}}, \mathbf{p}^{\text{jet}}) = \sum_i (E^i, p_x^i, p_y^i, p_z^i), \tag{2.34}$$

$$p_T^{\text{jet}} = \sqrt{(p_x^{\text{jet}})^2 + (p_y^{\text{jet}})^2}, \tag{2.35}$$

$$y^{\text{jet}} = \frac{1}{2} \ln \frac{E^{\text{jet}} + p_z^{\text{jet}}}{E^{\text{jet}} - p_z^{\text{jet}}}, \qquad \phi^{\text{jet}} = \tan^{-1} \frac{p_y^{\text{jet}}}{p_x^{\text{jet}}}. \tag{2.36}$$

The reason for using rapidity is that the recombination scheme leads to massive jets in Run II.

The algorithm may be very expensive computationally (considering about 6000 starting points for $\Delta y(\eta) \times \Delta\phi = 0.1 \times 0.1$ covering of the $y(\eta) \times \phi$ plane, with the $y(\eta)$ coverage of $\pm$ 5). Seed-based cone algorithm can be much more efficient in CPU time. Let us arrange the detector towers according to descending E_T and consider only those tower, passing a seed cut,

$$E_T^{\text{tower}} > E_T^{\text{seed}} \tag{2.37}$$

as starting points for the initial jet cones. The seed threshold E_T^{seed} must be chosen low enough so that variations of E_T^{seed} lead to negligible variations in any observable under consideration. The disadvantage is, however, the sensitivity to both infrared and collinear effects. The sensitivity to soft radiation can be removed by adding of 'midpoints' at the position given by $p_i + p_j, p_i + p_j + p_k$ etc. to the list of starting seeds. This scheme is used under the name ILCA (Improve Legacy Cone Algorithm) at DØ.

The main problem of the whole class of cone algorithms is the cone overlapping. In the definition there is nothing that will prevent the particle to belong to two (or more jets). In order to get rid of this another splitting or

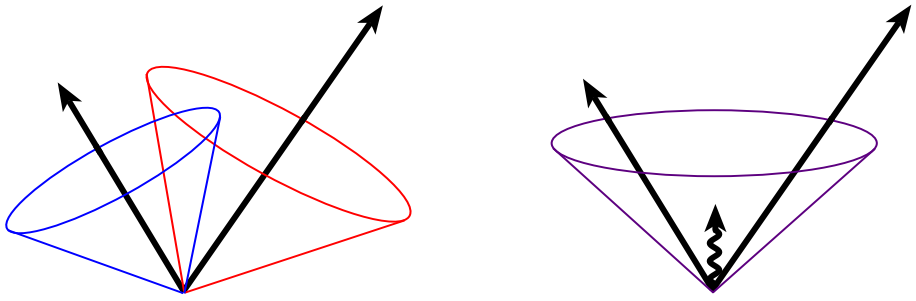

Figure 2.2: An illustration of infrared sensitivity in cone jet algorithm. Seeds are represented as arrows. Without soft radiation seeds will form two only slightly overlapped jets (left), while after a soft radiation they will be merged together (right).

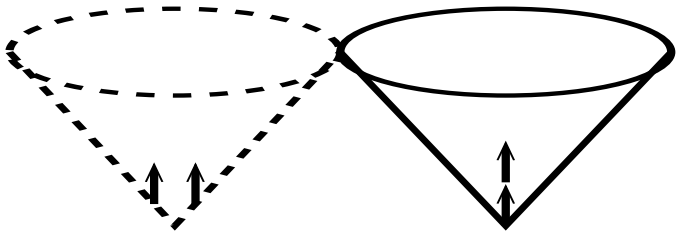

Figure 2.3: An illustration of collinear sensitivity in seed-based algorithm. Particles on the left will fail to form a seed because their energy is too much separated among detector cells. The configuration on the right will produce a seed because its energy is more narrowly distributed.

merging specifications have to be added to the algorithm. These specification will describe under which condition the jets will be merged together or splitted so they will no longer overlap.

General proposition for splitting and merging is that two jets will be merged if they share more than 50% of the transverse energy of the lower E_T jet. Otherwise overlapping jets will be splitted with the shared particles individually assigned to the jet that is closest in $y \times \phi$ space.

2.5.2 K_T Algorithm

The second main class of jet algorithms is the K_T ($k_T, k_\perp$ or Durham algorithm). The K_T algorithm starts with a list of so-called preclusters which are formed from calorimeter cells, particles or partons. The K_T for N particles is an N^3 algorithm. The preclustering therefore reduces the number of initial particles for time efficiency and also reduces the dependence on detector properties (cell type, their number or size). Each precluster is then assigned a fourvector

$$(E, \mathbf{p}) = E(1, \cos\phi \sin\theta, \sin\phi \sin\theta, \cos\theta), \tag{2.38}$$

where E is the energy associated with the precluster and ϕ, θ are the usual angles. For each precluster, the square of the transverse momentum, p_T^2 and the rapidity y is calculated

$$p_T^2 = p_x^2 + p_y^2, \qquad y = \frac{1}{2} \ln \frac{E + p_z}{E - p_z}. \tag{2.39}$$

The preclusters than form the jets in a following way:

1. For each precluster i define

$$d_i = p_{T,i}^2, \tag{2.40}$$

   and for each pair (i, j) of preclusters $(i \neq j)$, define

$$d_{ij} = \min(d_i, d_j) \frac{(y_i - y_j)^2 + (\phi_i - \phi_j)^2}{D^2}, \tag{2.41}$$

   where $D \approx 1$ is a parameter of the algorithm. For $D = 1$ and small angular differences of the preclusters $(y_i - y_j)^2 + (\phi_i - \phi_j)^2) \ll 1$, d_{ij} is the relative transverse momentum $k_\perp$ (squared) of one vector with respect to the other, whence the name of the algorithm.

2. Find the minimum of all the d_i and d_{ij} and label it d_{min}.

3. If d_{min} is a d_{ij}, remove preclusters i and j from the list and replace them with a new precluster $(E_{ij}, \mathbf{p}_{ij})$ given by

$$E_{ij} = E_i + E_j, \qquad \mathbf{p}_{ij} = \mathbf{p}_i + \mathbf{p}_j. \tag{2.42}$$

4. If d_{min} is a d_i, the corresponding precluster i is removed from the list of preclusters and added to the list of jets.

5. If any preclusters remain, repeat from step 1.

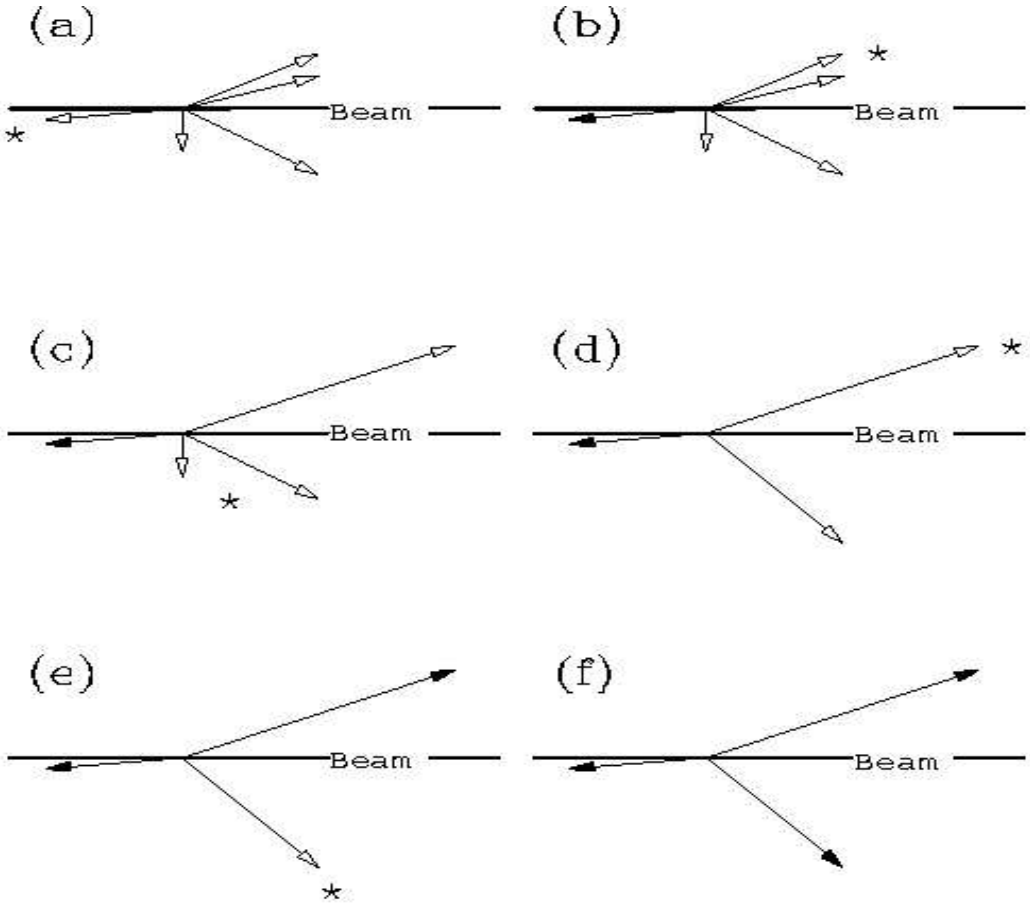

Figure 2.4: A simplified example of the K_T algorithm. The open arrows represent the original preclusters, and the solid arrows are the final state jets.

As in the case of the cone algorithm, there exist more possible modifications. The main differences (without considering detector dependent preclustering) are in the recombination scheme in step 3 and in the method of terminating the clustering. The end of clustering can be changed with

introducing a stopping parameter, $d_{\rm cut}$, that defines the hard scale of the physics process and separates the event into a hard scattering part (interesting to us) and a low-p_T part (beam or remnant jets from the rest of proton and antiproton).

Although the K_T algorithm should behave better than the Cone, a full program for it at hadron-hadron colliders had not yet been developed.

3 Tevatron and DØ

This section will cover a description of the Tevatron accelerator and the DØ detector. DØ is one of the two large general multi-purpose detectors at the Tevatron proton-antiproton collider (together with CDF) at the Fermi National Accelerator Laboratory (Fermilab, FNAL) near Chicago. The Tevatron, with it's circumference of 6.28 km, and particle collisions with a center-of-mass energy of 1.96 TeV, is currently the world's largest and most energetic accelerator.

The Tevatron is the last accelerator in a accelerating complex used at Fermilab. The complex starts with the Cockcroft-Walton preaccelerator which accelerates H^- ions to 750 keV. These ions are then accelerated in Linac (linear accelerator) to 400 MeV. Then the hydrogen ions are stripped of the electrons and the protons are accelerated to 8 GeV in the Booster synchrotron and then injected to the Main Injector. Here are the protons accelerated to 120 or 150 GeV. 120 GeV protons are used in the Antiproton Source to create and accelerate antiprotons. These are then injected back to the Main Injector. Beams of protons and antiprotons with 150 GeV are finally injected into Tevatron.

The beams in the Tevatron are not steady flows of particles. The protons and antiprotons are localized in bunches. Currently used number of bunches is 36 for protons and 36 for antiprotons. There are three superbunches within the turn, each consisting of 12 bunches. Within a superbunch, bunches are separated by 396 ns, which means that the superbunches are approximately 4.36 μs long and the gap between superbunches is 2.6 μs. Taking this together, 3 superbunches with 4.36 μs and three gaps with 2.6 μs, one gets approximately 21 μs and that is the time it takes particles moving at the speed of light to make one turn in the Tevatron (the circumference divided

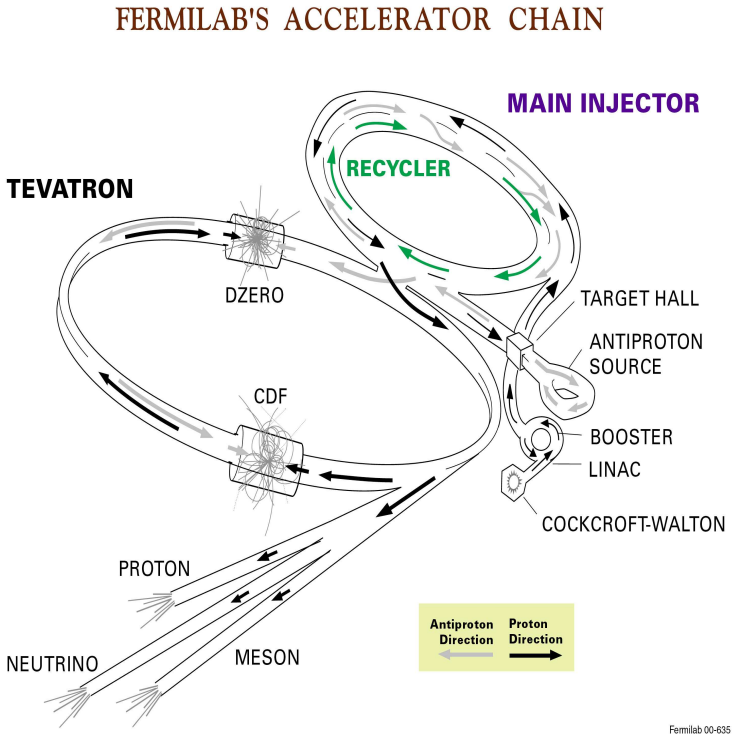

Figure 3.1: Schematic view of the accelerator complex

by the speed of light). The Tevatron was designed and is operated the way that the collisions can happen only at DØ and CDF. The bunches are spaced that way that DØ (also CDF) sees 36 collisions of bunches per the evolution.

3.1 DØ Detector

The DØ experiment was built in late eighties. Between years 1992 and 1996 the data were taken for the first time. One of the main results was the observation of the top quark in 1995. In 1996 the DØ started an upgrade to be able to run at the new accelerator conditions. The upgraded versions of the Tevatron and the detectors (called Run II) have started their operation in March 2001.

The scheme of the detector is displayed in figure 3.2. From the interaction point it is formed by a series of different subdetectors. The first one is

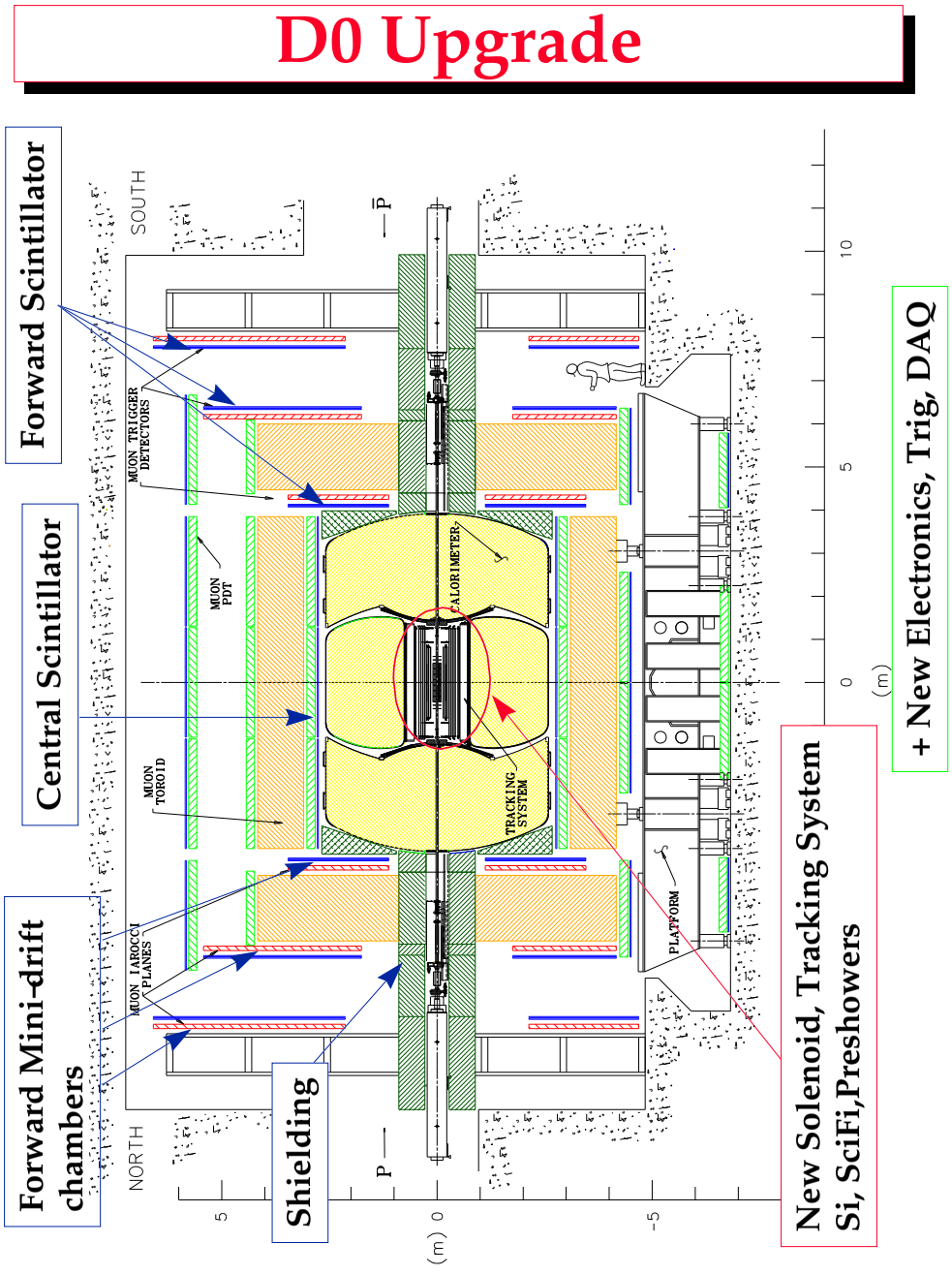

Figure 3.2: Overview of the DØ detector

the tracking system. It consists of the Silicon Microstrip Tracker (SMT) and the Central Fiber Tracker (CFT) placed in the 2T magnetic field. The SMT consists of silicon disks and barrels formed into 6 disk/barrel modules. Each barrel module consists of 4 (radial) layers of detector ladder assemblies. Layers one and three are single sided silicon microstrip detectors and layers two and four are double sided with 2-degree stereo angle. Each disk module has 12 wedge shaped double-sided detectors with a 30 degree stereo angle. There are also three sets of end disks on each side. A scintillating fiber tracker surrounds the silicon detector. The CFT consists of about 74000 scintillating fibers mounted on eight concentric cylinders. The curvature of the charged particle tracks allows us to determine particle transverse momenta for all charged particles within the range $|\eta| < 2.0$ (for definition of the coordinate system see Section 3.2). The tracks are also used to reconstruct primary and secondary vertices in the interaction. They also help with particle identification.

The Central Preshower (CPS) and the Forward Preshower (FPS) detectors are placed between the magnet and the calorimeter. They are designed to enhance the electron and photon identification. Next there are three main parts of the calorimeter: the central cryostat (CC) and two end-cap cryostats (EC). The space between the cryostats is filled by the Inter-Cryostat Detector (ICD) and Massless Gap Detector (this place is defined with $0.8 < |\eta| < 1.5$. The calorimeter comprises of the electromagnetic part capturing electrons and photons and of the hadronic part capturing hadrons. The calorimeter is an essential tool for jet detection.

High energetic muons are able to penetrate through calorimeter. They are detected by the muon system which surrounds all the subdetectors. The Forward Proton Detector (FPD) is a new detector dedicated to diffractive physics in Run II. The FPD tracks the protons and anti-protons that were scattered at very small angles. The detector is supplemented by the Luminosity Monitor (LM) detector designed to measure the luminosity. Another essential part is the detector read-out and trigger system. The DØ trigger system selects "interesting" events produced by the Tevatron for further offline analysis. The beam colliding frequency is about a few MHz. The trigger system selects 30-50 Hz of these events to be written to the tape. DØ has

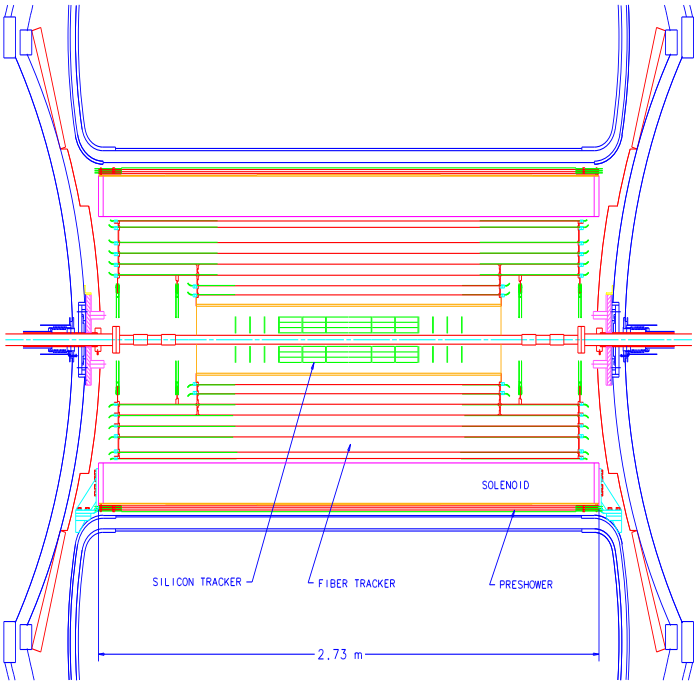

Figure 3.3: DØ Tracking system

three levels of trigger filtering:

Level 1 A pipelined hardware trigger with inputs from the calorimeter, scintillator counters, muon system and fiber tracker.

Level 2 L1 information is combined and extended in specialized preprocessors. It also adds information from the silicon tracker.

Level 3 A Linux processor farm which can reconstruct and analyze events.

3.1.1 Calorimeter

Calorimeter (in figure 3.4) is the main detector which enables the jet measurement. Its main task is to absorb deposited energy and measure the overall energy flow in the interaction. Calorimeter is a large bulk of material (uranium, copper, and steel in the case of the DØ calorimeter) that absorbs

the outgoing particles combined with an active medium (liquid argon in the case of the DØ) that samples the electromagnetic and hadronic showers. Almost all known elementary particles are captured inside. The calorimeter provides identification of electrons, photons, taus and hadronic jets. Muons are detected by the muon detectors behind the calorimeter and neutrinos are indicated by the overall transverse energy imbalance.

Calorimeter is formed by three parts - the central cryostat (CC) and two end-cap cryostats (EC). Each cryostat is divided longitudinally into three sections: the electromagnetic (EM), the fine hadronic (FH), and the coarse hadronic (CH). They are composed of small cells as building blocks. Typical cell size in terms of azimuthal angle ϕ and pseudorapidity η is $\Delta\phi \times \Delta\eta = 0.1 \times 0.1$. The cells are arranged into projective towers. The term projective means that the cell centers in the tower lie on the ray originating from the geometrical center of the detector (figure 3.5).

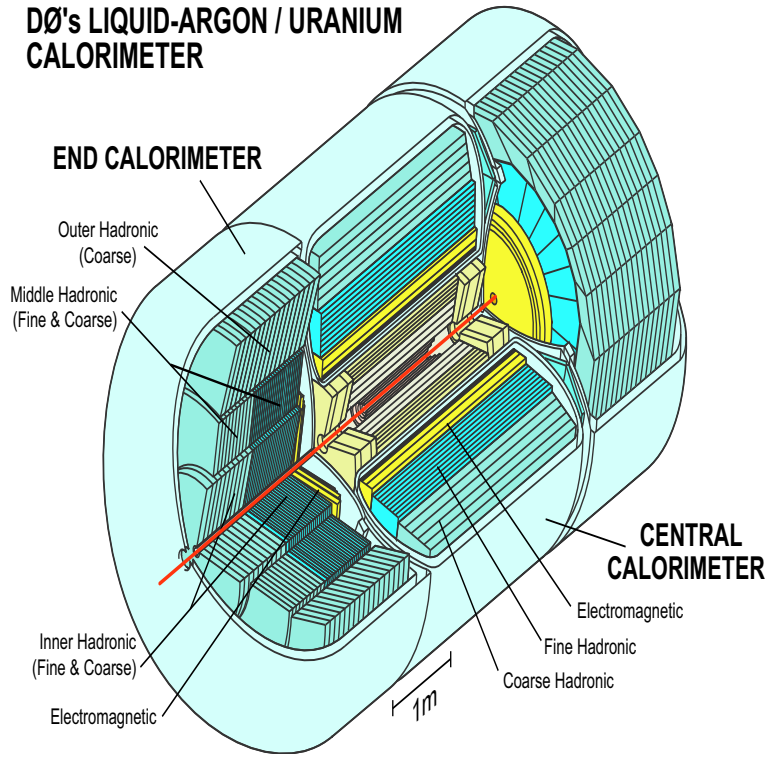

Figure 3.4: The DØ Calorimeter

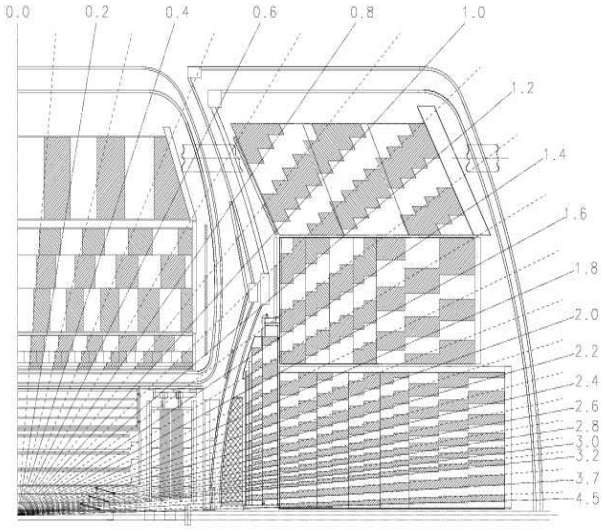

Figure 3.5: Layout of calorimeter cells and projective towers

3.2 Coordinate System

The coordinate system at DØ is defined in the following way. It is a right handed system with the z-axis increasing along the proton beam. The z-axis, and the origin of coordinates are defined to be centered in the CFT with y-axis pointing upwards. All distances are measured in cm. The azimuthal angle ϕ is defined to be in radians, $0 < \phi < 2\pi$, with $\phi = 0$ for $x > 0, y = 0$ and $\phi \in (0, \pi)$ for $y > 0$. The angle θ is given in radians from 0 to π. $\theta = 0$ for $x = y = 0$ and $z > 0$, $\theta = \pi$ for $x = y = 0$ and $z < 0$. Pseudorapidity η is defined as usual $\eta = -\ln\tan(\theta/2)$.

3.3 Data Taking

The store starts when the protons and antiprotons are finally injected into the Tevatron. This is a time period during the beams collide. If there are no problems, it can last from several hours to a few days. The store is divided into smaller sections called runs, where the data is collected. Runs do not usually last more than four hours, because parameters of data taking have to be changed as the beam parameters such as luminosity change.

3.3.1 Data Formats

Several file formats could be encountered during the analysis. The output of the detector are the RAW data. This output from Level 3 is about 500 kb per event. This data have to be reconstructed. The reconstruction is done by the DØ Offline Reconstruction Program (RECO). This is a CPU intensive program that processes either collider events recorded during online data taking or simulated events produced with DØ Monte Carlo program. The output from RECO is a format containing many so-called chunks associated with each type of reconstructed object (EM objects, jets, muons, etc.). RECO is designed to produce two output formats which can be used for physics analyses.

The Data Summary Tape (DST) contains all information necessary to perform any physics analysis, and is designed to be 150kb per event. The Thumbnail (TMB) contains a summary of the DST, and is designed to be 15 kb per event. The TMB can be used directly to perform many useful analyses.

Although the analysis can be done at the DST or TMB level, in this thesis another format is used. The DST or TMB files are reprocessed once more by the D0ChunkAnalyze program to produce final ROOT files. These ROOT files can be then analyzed using the C/C++ programing and graphical interface of ROOT [38].

4 Data Analysis

The data used in this thesis were recorded between the end of April 2002 and September 2003. Only data corresponding to trigger versions 8.20 - 12 were considered. The events were reconstructed with various version of p14 release of the DØ reconstruction software (d0reco). The p13 version data were re-reconstructed from DST files with p14.05.02-p14.06.00 versions, p14.03 and p14.05.00 versions were fixed on thumbnail level with *fixtmb.01* and *fixtmb.02* respectively. After the thumbnail fixing, all data are compatible with p14.06 release. For the associated lepton production, used data is a subset of the jet studies data.

Run list provided by A. Kupčo is used to analyze only runs marked as good in Run Quality Database.

4.1 Event Selection

Sample used in this thesis satisfies the following event selection criteria.

- **Topological cuts**

  - event contains at least two jets reconstructed with the Run II Cone algorithms with a cone size of $R = 0.7$ as specified in Section 2.5.1. This cut is used to perform inclusive dijet analysis.

- **Kinematical cuts**

  - uncorrected transverse momentum of the second leading jet has to be above 40 GeV (to consider high-p_T events only).

- **Event quality cuts**

  - event has to fire one of JT_25TT_NG, JT_45TT, JT_65TT, or JT_95TT jet triggers. Consequences of this cut will be discussed later in the Data Analysis section.
  - both p_T-leading jets have to pass the standard jet selection criteria (specified below),
  - cut on missing E_T: $\not\!\!E_T < 0.7 p_T^{\mathrm{jet1}}$, where p_T^{jet1} is uncorrected transverse momentum of the leading jet,
  - primary vertex has to have at least three associated tracks,
  - z coordinate (along beam axis) of the primary vertex is within 50 cm from the origin of the coordinate system: $|z_{\mathrm{vtx}}| < 50\,\mathrm{cm}$,
  - additionally events containing unphysical amount (> 1.96TeV) of energy were not considered.

The following jet quality criteria are used to determine good jets.

- **Electromagnetic fraction (EMF):** Jets are required to have electromagnetic fraction $0.05 <$ EMF< 0.95 (fraction of jet E_T deposited in EM layers of the calorimeter). This cut can however introduce an inefficiency for good jets at high p_T.

- **Coarse hadronic fraction (CHF):** A cut on coarse hadronic fraction is necessary because of the high noise in these layers of the calorimeter. Jets are required to have CHF < 0.40. This cut can be also less efficient for very high p_T jets where more energy is deposited in the coarse hadronic part.

- **Hot cell fraction (HotF):** This cut removes the jets built because of hot cell inside the calorimeter (a cell showing too much energy but low occupancy). The fraction is counted as the ratio of the transverse energy stored in the leading cell to the second leading cell in the jet, and is required to be HotF < 10.

- **n90:** This variable is used to remove hot towers in the calorimeter. The towers in the jet are ordered in transverse energy, and the towers that comprise at least 90% of the jet transverse energy are counted. The requirement is n90 > 1 (i.e. jets with 90% of transverse energy formed by only one tower are removed).

- **Level 1 confirmation:** Confirmation from the L1 readout is required for the p14 data. Scalar transverse energy L1SET, computed from the L1 calorimeter towers in the $R = 0.5$ cone in the direction of the jet, is used for this purpose. L1SET $> 0.4 p_T^{\text{jet}}(1 - \text{CHF})$ for the CC or EC part of the calorimeter, L1SET $> 0.2 p_T^{\text{jet}}(1 - \text{CHF})$ for the ICD or L1SET $> 80\,\text{GeV}$.

- **f90:** For runs < 172359 the L1 calorimeter readout was available only up to $|\eta_{\text{DET}}| = 2.4$. Starting from run 172359 the readout was extended up to $|\eta_{\text{DET}}| = 3.2$. Outside this regions one has to relay on old jet ID cut using the f90 variable. f90 is the n90 variable divided by the total number of calorimeter towers in the jet. Good jets are required to have f90 < 0.5 or CHF < 0.15.

- **Detector pseudorapidity (η_{DET}):** Good jets are required to have $|\eta_{\text{det}}| < 3.4$. Detection at these angles is more difficult and less accurate than at angles defining the central region. Also Jet Energy Scale corrections are not certified at large angles.

Jet energies and momenta were corrected using jetcorr package v05-02-00. These corrections are applied to get the real jet energy and momenta before entering the detector. They consist of some offset O because of calorimeter noise, response of the calorimeter to the jet R_{jet} and showering S representing portion of jet energy deposited outside the cone. The final relation is:

$$E^{\text{jet}}_{\text{particles}} = \frac{E^{\text{jet}}_{\text{detector}} - O}{R_{\text{jet}} \cdot S}. \tag{4.1}$$

Correction factor for energies and momenta is then

$$\text{Corrf} = \frac{E^{\text{jet}}_{\text{particles}}}{E^{\text{jet}}_{\text{detector}}}. \tag{4.2}$$

Due to the geometry of the calorimeter these corrections also depend on the pseudorapidities (angles) of jets.

4.2 Cut Results

All used cuts are normal cuts used in usual DØ jet analysis. Therefore their efficiency is not studied in this thesis. Plots 4.1, 4.2 and 4.3 summarize which events were cut out. Table 4.1 shows, how many events were cut out in each step of cutting.

Initial number of events	24708202
Old trigger version	1257608
Bad run	781653
Duplicated events	1594261
Without required jet trigger	3808970
Less than 2 jets	162588
Low p_T jets	7909696
High $\not\!\!E_T$	560914
Primary vertex	1515305
EMF out of range	207786
CHF > 0.4	211330
HotF> 10	16564
n90	194
L1 confirmation / f90	120377
Detector rapidity	0
Other	561
Remaining events	6560395

Table 4.1: Number of events cut out at different stages of cutting. First line showing the initial number of events in sample. Next lines showing how many events were cut out from the remaining sample.

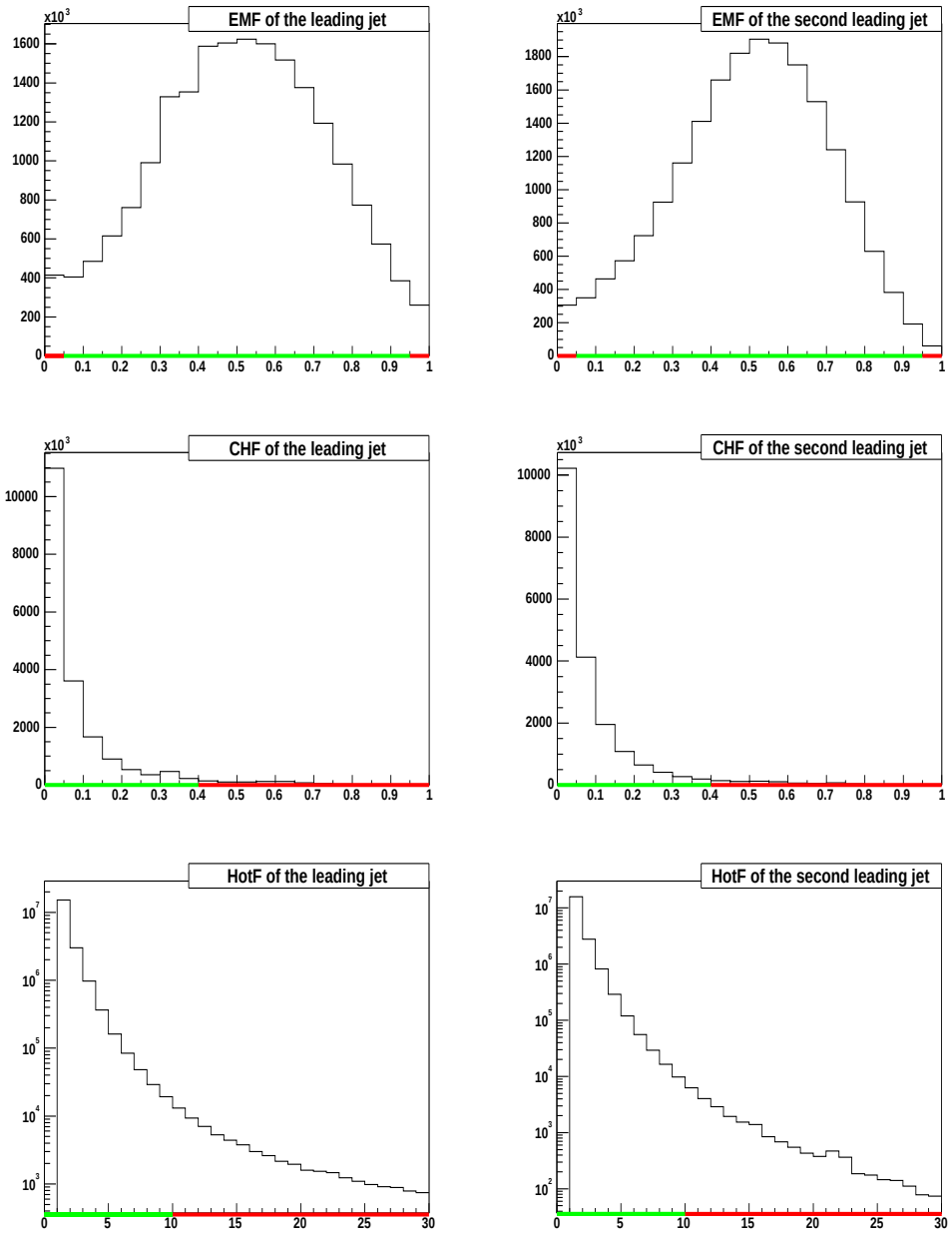

Figure 4.1: Cuts on EMF, CHF and HotF represented by red and green lines. Red lines show rejected regions.

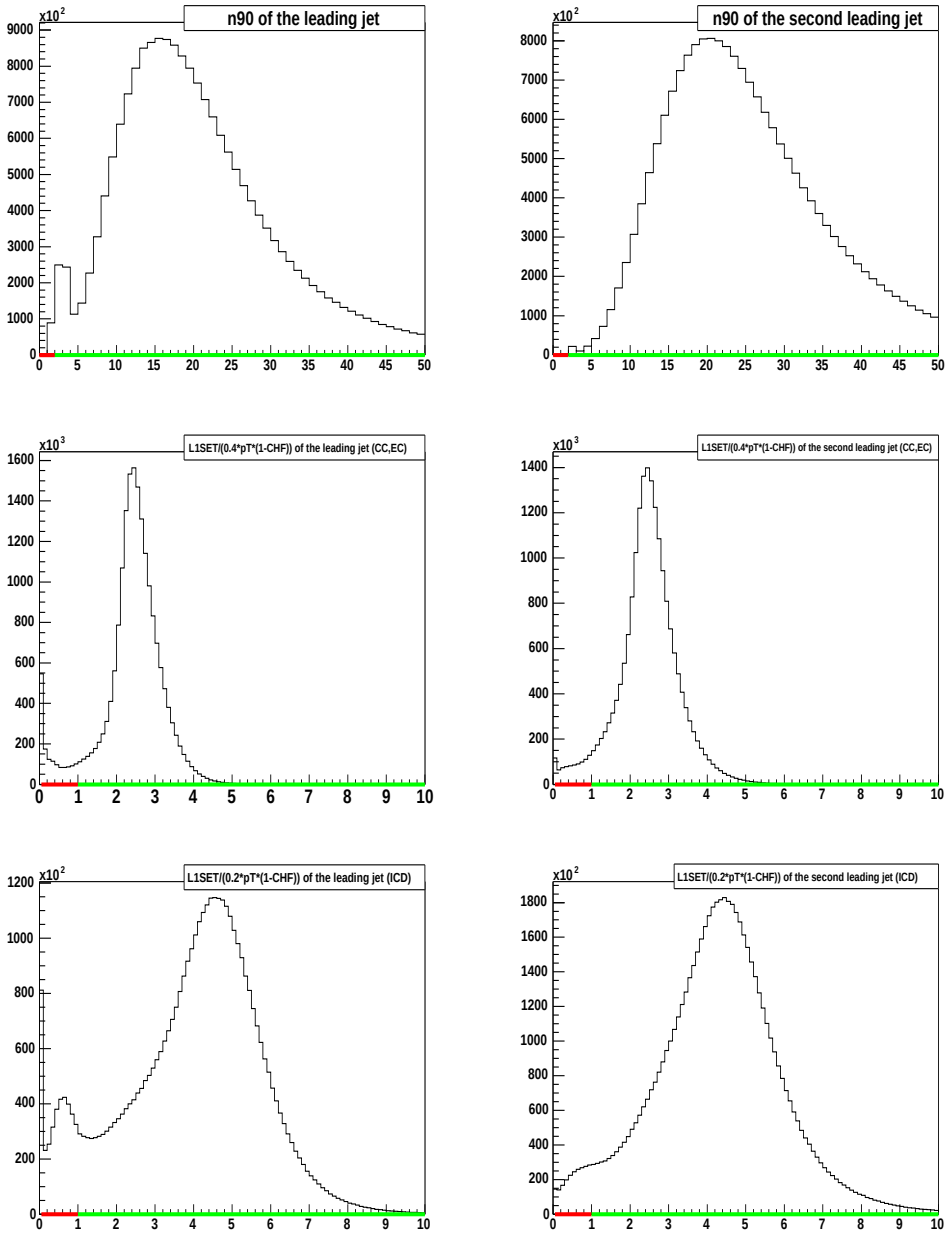

Figure 4.2: Cuts on n90 and L1 confirmation represented by red and green lines. Red lines show rejected regions. However not all jets with L1SET=0 are not removed, because they should belong to large pseudorapidity jets, which are then tested for f90 variable.

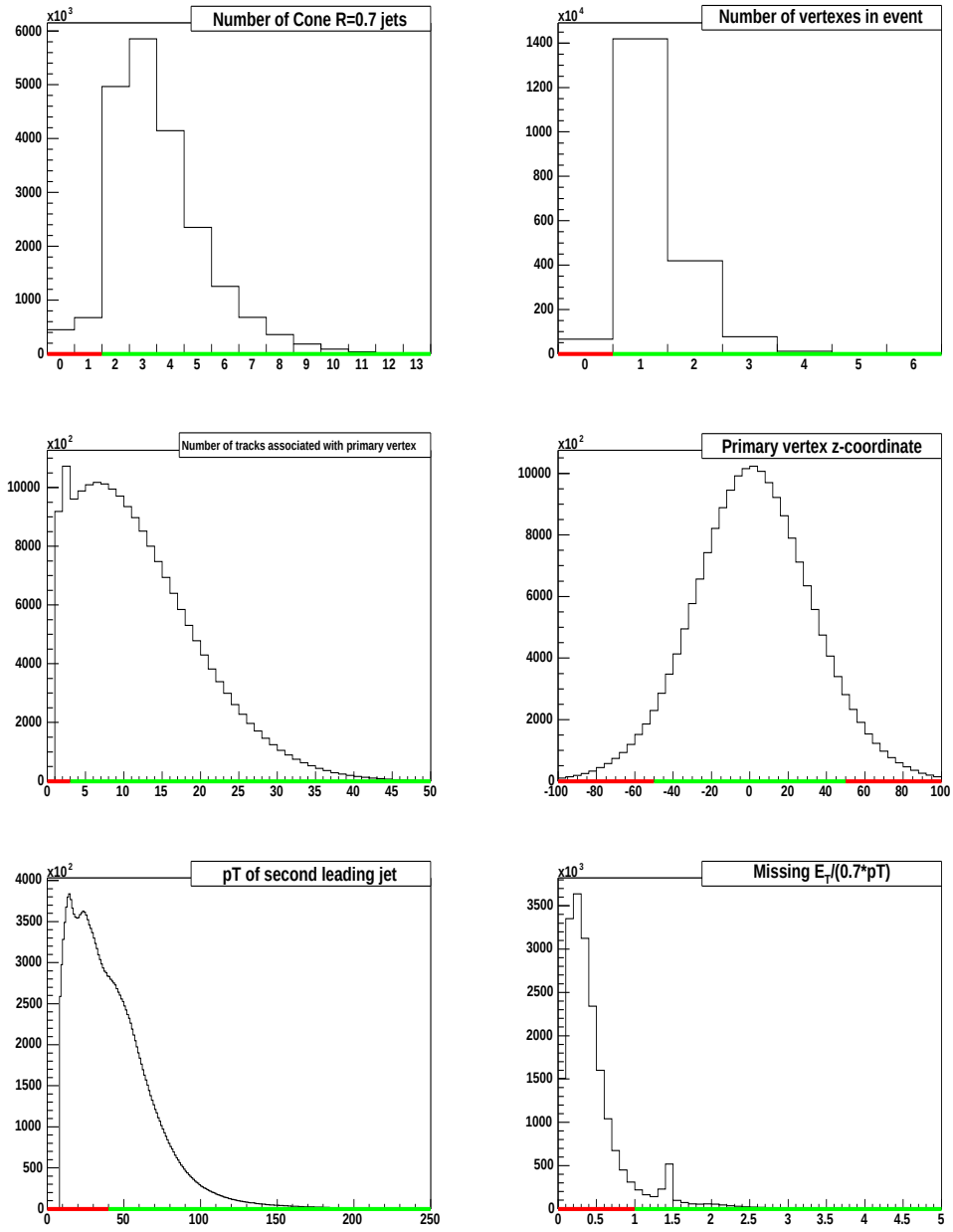

Figure 4.3: Cuts on number of jet and primary vertex properties, and on $\not\!\!E_T$ represented by red and green lines. Red lines show rejected regions.

4.3 Jet Analysis

In this thesis inclusive dijet production is investigated. Inclusive process means interaction of type:

$$p + \overline{p} \rightarrow 2\,\text{jets} + X, \tag{4.3}$$

where X could be another jets, electrons, muons, ...

The events are required to fire a trigger (one of JT_25TT_NG, JT_45TT, JT_65, JT_95TT jet triggers). These triggers have special requirements on each level of the trigger system (briefly reviewed in table 4.2). Special interest is given to high-p_T events, however low-p_T events occur in higher frequencies. This problem is solved by prescaling. It means that lower jet trigger is fired only once while more events satisfy its requirements. This helps to keep the L3 frequency low enough to be able to record all interesting events. To be able to present result in lower p_T regions with the right frequencies, one has to multiply the number of events with a prescale factor. The prescale factors for the chosen triggers are shown in table 4.3. They are only approximate numbers and are taken from reference [29]. The study of the trigger efficiencies, if the right trigger was fired, is not performed.

Trigger	L1 (>5 GeV)	L2 (GeV)	L3 (GeV)
JT_25TT_NG	2 towers	none	1 jet with $E_T > 25$
JT_45TT	2 towers	none	1 jet with $E_T > 45$
JT_65TT	3 towers	1 jet with $E_T > 20$	1 jet with $E_T > 65$
JT_95TT	4 towers	1 jet with $E_T > 30$	1 jet with $E_T > 95$

Table 4.2: A summary of jet trigger requirement on each level of the trigger system

4.3.1 Overall Jet Properties

Tevatron produces collisions at center-of-mass energy $\sqrt{s}$ of 1.96 TeV. The whole energy does not usually take part in the hard scattering process. H_T

variable computed as a sum of jet transverse energies is used as a signature of heavy object created in the collision.

$$H_T = \sum_{\text{jet}} E_{T_{\text{jet}}}, \tag{4.4}$$

with transverse energy

$$E_T = E \sin\theta. \tag{4.5}$$

It is used as a cut when studying for example top-quark properties. All jets in the event are required to satisfy the jet quality criteria. Distribution of H_T is shown in figure 4.4 together with the distribution of a number of cone $R = 0.7$ jets.

Properties of all good jets in the sample are summarized in figure 4.5.

The angular plots show overall uniform distribution of jets. The uniformity in ϕ confirms that there is not a preferred direction of jet production in x-y plane. The η distribution shows the overall parton scattering properties. This will be more studied in the dijet inclusive state.

Transverse momentum p_T also informs about hardness of the process. It is a module of the jet momentum transverse to the beam axis ($p_T = \sqrt{p_x^2 + p_y^2}$). The p_T distributions for the leading and the second leading jets are shown in figure 4.6.

4.3.2 Dijet properties

The dijet analysis is performed on first two p_T leading jets. These jets are needed to satisfy the jet quality criteria described in section 4.1.

Trigger	Prescale factor
JT_25TT_NG	150
JT_45TT	4.7
JT_65TT	1.3
JT_95TT	1

Table 4.3: Prescale factors

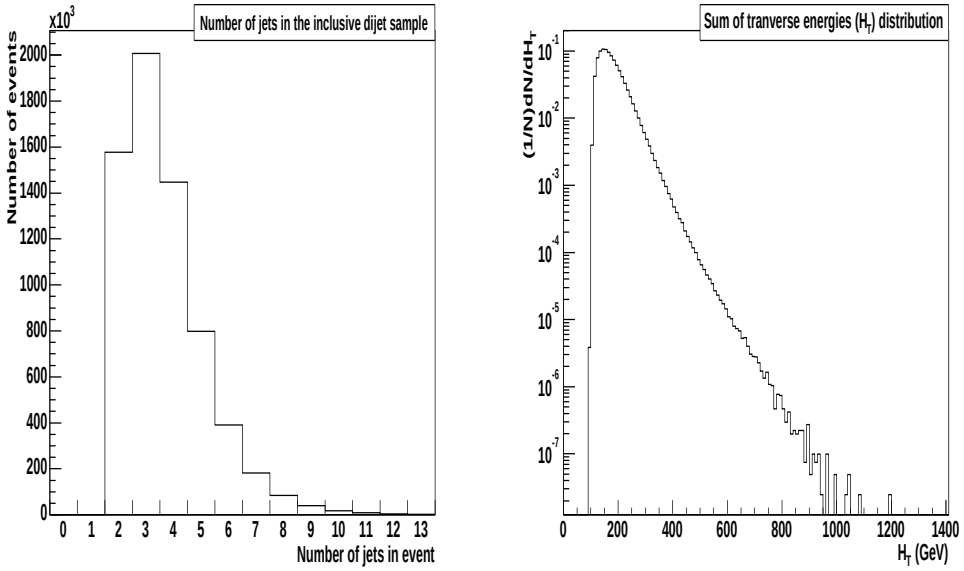

Figure 4.4: Distribution of number of jets in the final sample (left, without trigger prescale factors) and sum of the jet transverse energie

The angular distribution of the jet momenta and distribution of dijets in the detector is shown in figure 4.7.

Due to four-momentum conservation, the dijet mass,

$$M_{JJ}^2 = (E_{\text{jet1}} + E_{\text{jet2}})^2 - (\vec{p}_{\text{jet1}} + \vec{p}_{\text{jet2}})^2, \tag{4.6}$$

specifies the properties of the parton interaction. While single jet production is usually studied using the p_T distribution ($\mathrm{d}\sigma/\mathrm{d}p_T$), the dijet production is characterized with the invariant mass ($\mathrm{d}\sigma/\mathrm{d}M_{JJ}$). The dijet mass distribution is shown in figure 4.8.

Jet angles are given in the coordinate system defined by the detector. However, when transformation to the center of mass of the interacting partons is performed, one can study at which angles jets were produced. However it is a tricky task. While the general transformation to the center of mass system of the two jets could be done, there is an arbitrary way, how to choose the initial direction of the partons. One can accept an approximation. Considering the partons moving only in the z coordinate and perform

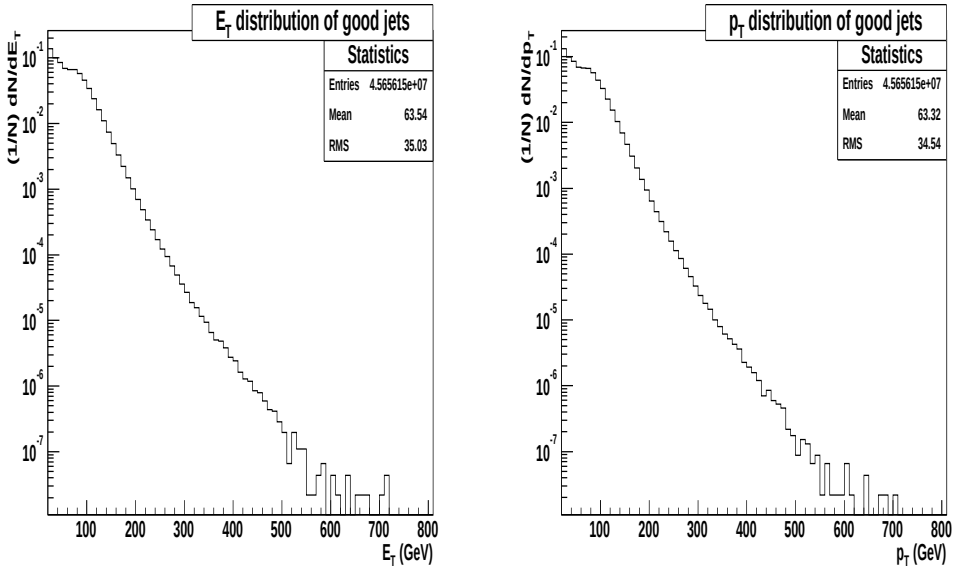

Figure 4.5: Summary of good jet properties (jets satisfying jet quality criteria). Plots show E_T (left) and p_T of the jets. The difference between them is given by the recombination scheme used in the ILCA cone algorithm in Run II. The jets in Run I were massless causing $E_T = p_T$.

the transformation to the center of mass system as Lorentz boost in the z direction only. This boost is a such one, where both jets have the same angle with the z-axis.

The Lorentz boost in given direction can be written as:

$$E' = \gamma(E - \beta p_L) \tag{4.7}$$

$$p'_L = \gamma(p_L - \beta E), \tag{4.8}$$

$$p'_T = p_T, \tag{4.9}$$

with p_L the module of the projection of momentum on the boost direction and p_T the orthogonal part to the p_L. Also $\gamma = (1 - \beta^2)^{-1/2}$ and β given from the requirement on the angles in the boosted frame. The condition on angles can be formulated as (numerical labels mean the first and the second jet)

$$-\frac{p'_{L1}}{p'_{T1}} = \frac{p'_{L2}}{p'_{T2}}. \tag{4.10}$$

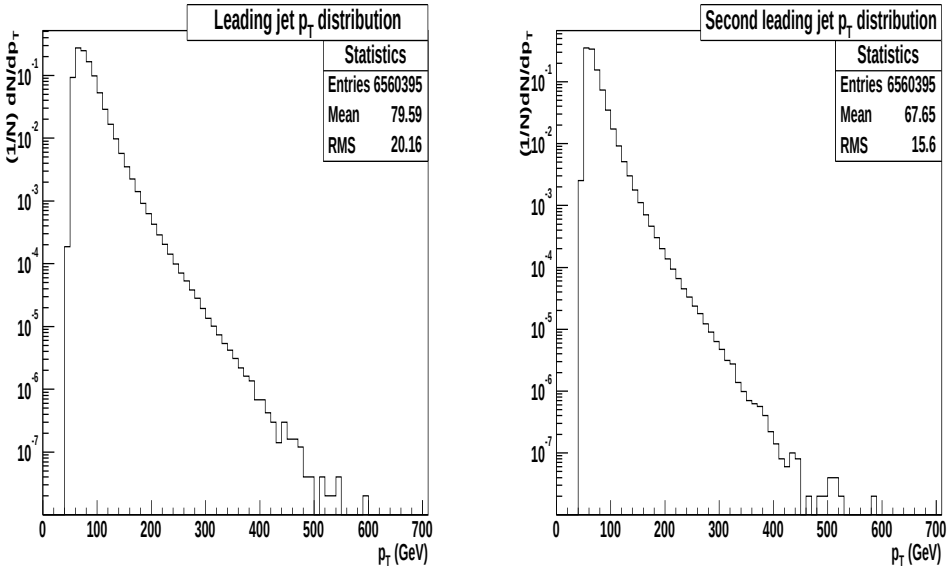

Figure 4.6: Transverse momenta distribution. Plots show p_T distribution of the leading (on the left) and second leading jet. Most energetic jets have transverse momentum of a few hundred GeV.

Using eq. (4.8) one gets

$$\beta = \frac{p_{T1}p_{L2} + p_{L1}p_{T2}}{E_1 p_{T2} + p_{T1}E_2}. \tag{4.11}$$

Due to the factorization theorem, hadronical cross-section can be written as

$$\sigma^{p\overline{p}\to X} = \sum_{i,j} \int f_i(x_1) f_j(x_2) \mathrm{d}x_1 \mathrm{d}x_2 \sigma^{\mathrm{parton}}, \tag{4.12}$$

where σ^{parton} represents cross-section for process where partons i and j form final state X. For the $\cos\theta^\star$ dependence, the eq. (4.12) can be formulated as

$$\frac{\mathrm{d}\sigma^{p\overline{p}\to X}}{\mathrm{d}\cos\theta^\star} = \sum_{i,j} \int f_i(x_1) f_j(x_2) \mathrm{d}x_1 \mathrm{d}x_2 \frac{\mathrm{d}\sigma^{\mathrm{parton}}}{\mathrm{d}\cos\theta^\star}. \tag{4.13}$$

Partonic cross-sections can be computed by QCD. Cross-section for $2 \to 2$ parton interaction is given by

$$\frac{\mathrm{d}\sigma}{\mathrm{d}t} = \frac{\overline{|M|}^2}{16\pi s^2}. \tag{4.14}$$

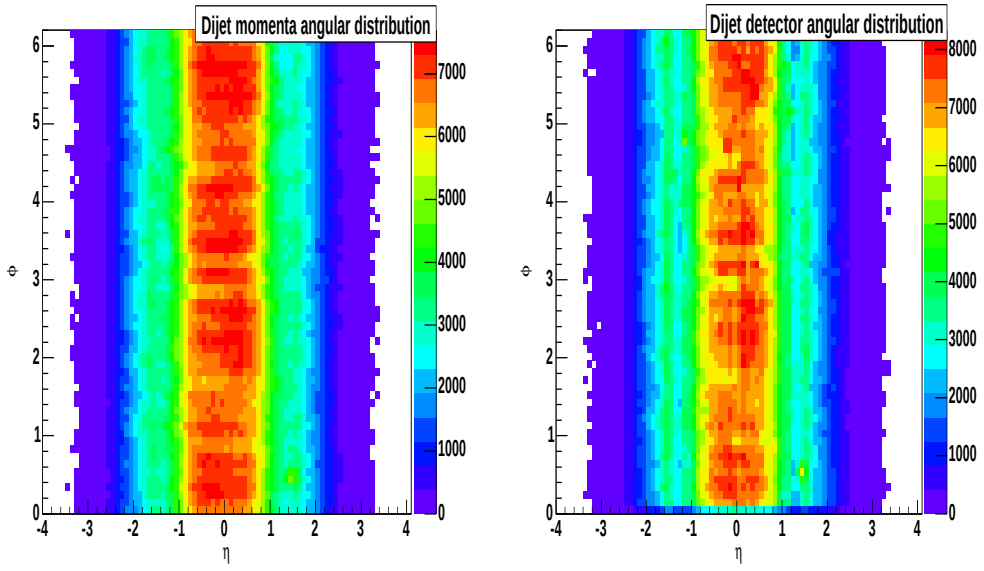

Figure 4.7: Dijet angular distributions. Plot on the left shows the angular distribution of the jet momenta as 3-vectors. Plot on the right shows the detector (calorimeter) angular distribution. The difference is given by the vertex position.

Mandelstam variables t and u can be written in the center-of-mass system as

$$t = -\frac{s}{2}(1-\cos\theta), \tag{4.15}$$

$$u = -\frac{s}{2}(1+\cos\theta). \tag{4.16}$$

At fixed center-of-mass total energy s, $\mathrm{d}t$ simplyfies to

$$\mathrm{d}t = \frac{s}{2}\mathrm{d}\cos\theta, \tag{4.17}$$

and thus

$$\left.\frac{\mathrm{d}\sigma}{\mathrm{d}\cos\theta}\right|_s = \frac{\overline{|M|}^2}{32\pi s}. \tag{4.18}$$

Partonic angular dependence is nearly identical (up to multiplication factor) for all quark and gluon processes. Therefore all these processes are approximated by the $gg \to gg$ interaction. Matrix element for this process is taken

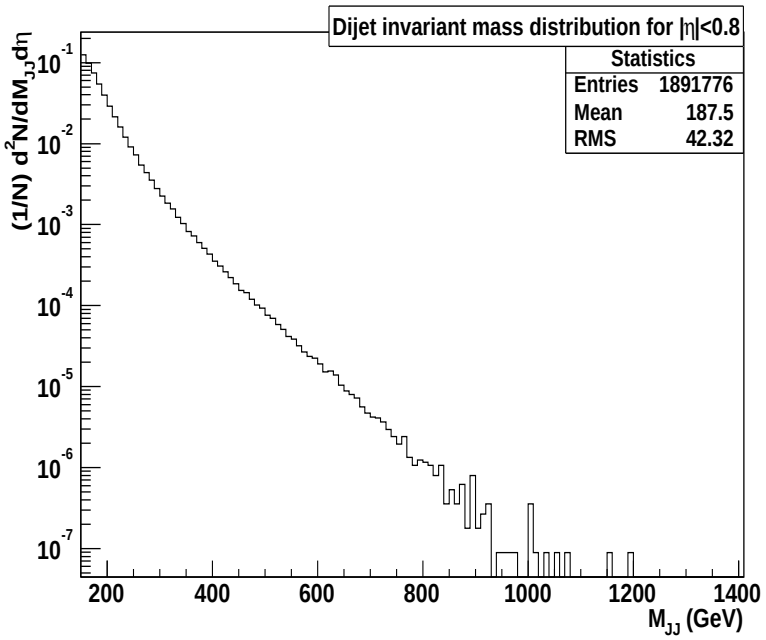

Figure 4.8: Dijet invariant mass distribution in the $|\eta_{\mathrm{DET}}| < 0.8$ region.

from reference [7] and reads (without coupling constant)

$$|M| = \frac{9}{2}(3 - \frac{tu}{s^2} - \frac{su}{t^2} - \frac{st}{u^2}). \tag{4.19}$$

Summing over all possible partons and integrating over parton distributions is taken together with the coupling constant and the total energy as a multiplication factor. Therefore the angular distribution should behave as

$$\frac{\mathrm{d}\sigma^{p\overline{p}\to 2\mathrm{jets}}}{\mathrm{d}\cos\theta^\star} = C_1 * \left(3 - \frac{1-\cos^2\theta^\star}{4} + 2\frac{1-\cos\theta^\star}{(1+\cos\theta^\star)^2} + 2\frac{1+\cos\theta^\star}{(1-\cos\theta^\star)^2}\right). \tag{4.20}$$

However the total fourmomentum s is not fixed. This variable is at the parton level represented by the dijet mass. To correct this effect, three different energy bins are used corresponding to dijet mass intervals of (0-300 GeV, 300-600 GeV, 600- GeV). This changes the differential cross-section to double differential. Also the eq. (4.20) corresponds to ideal case (or high-energy limit), therefore it is corrected for background. This background is taken

isotropic in $\cos\theta^\star$. The final fit is performed as

$$\frac{\mathrm{d}^2\sigma^{p\bar{p}\to 2\mathrm{jets}}}{\mathrm{d}M_{JJ}\mathrm{d}\cos\theta^\star} = C_0 + C_1 * \left(3 - \frac{1-\cos^2\theta^\star}{4} + \frac{2-2\cos\theta^\star}{(1+\cos\theta^\star)^2} + \frac{2+2\cos\theta^\star}{(1-\cos\theta^\star)^2}\right). \tag{4.21}$$

The angular distribution of $|\cos\theta^\star|$ given by the jet momentum and the z-axis in the boosted frame for the different dijet mass regions is shown in figures 4.9, 4.10 and 4.11.

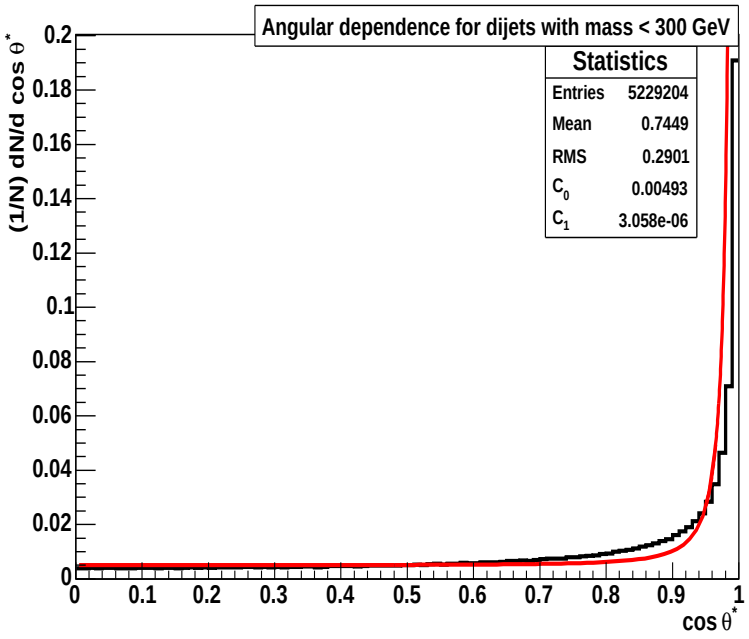

Figure 4.9: Distribution of $\cos\theta^\star$ for dijet invariant mass lower than 300 GeV in the frame where the angle between jet and z axis is identical for both jets.

4.4 Cross-sections and Measured Quantities

It is a fundamental property of quantum theories that only probabilities that something can happen can be given. On the opposite side, experiments also give statistical results. Large number of events is collected and the results are the mean numbers of the statistics. Usual quantities of nuclear and high-

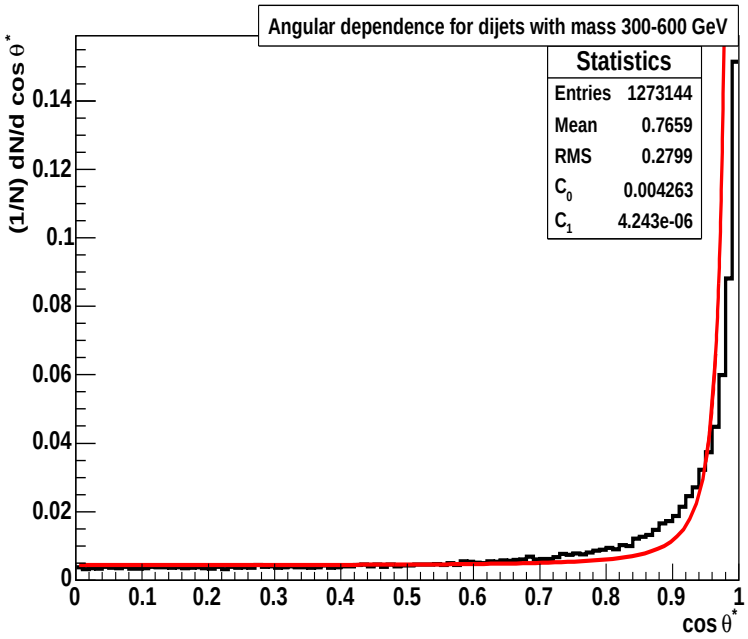

Figure 4.10: Distribution of $\cos\theta^\star$ for dijet invariant mass in the interval from 300 to 600 GeV in the frame where the angle between jet and z axis is identical for both jets.

energy physics are the cross-sections. They are computed from the observed distributions using the following formula:

$$\left\langle \frac{\mathrm{d}\sigma}{\mathrm{d}x} \right\rangle_{\mathrm{bin}} = \frac{N_{\mathrm{evt}}}{\mathcal{L}} \frac{1}{\epsilon_{\mathrm{eff}}} C_{\mathrm{unsmear}} \frac{1}{\Delta x}, \tag{4.22}$$

where N_{evt}, $\mathcal{L}$, ϵ_{eff}, Δx represent the number of events in the bin, luminosity (characterizing the total number of events), the jet and event cut efficiencies, the unsmearing (that only finite size bin are used instead of infinitesimally small ones) and the width of the bin, respectively. None of these factors are studied in this thesis. Therefore only normalized distributions of the type

$$\frac{1}{N}\frac{\mathrm{d}N}{\mathrm{d}x}, \qquad \frac{1}{N}\frac{\mathrm{d}^2N}{\mathrm{d}x_1\mathrm{d}x_2}, \qquad \dots \tag{4.23}$$

are shown.

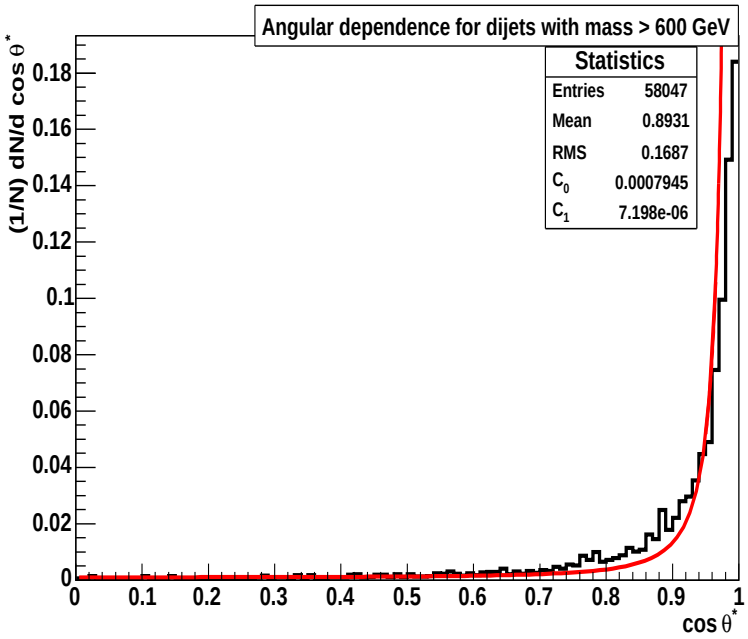

Figure 4.11: Distribution of $\cos\theta^\star$ for dijet invariant mass greater than 600 GeV in the frame where the angle between jet and z axis is identical for both jets.

The results must be complemented with errors. There are two kinds of errors. The first one is a statistical error given by the size of the sample, the second one is a systematic error given by different assumptions made during the analysis (including errors given by cuts, jet energy scale corrections and luminosity).

Another problem is that the theoretical prediction of divergences in the cross-sections. This is solved by showing differential cross-sections instead of absolute ones. When trying to get the integrated cross-sections, one has to introduce cut-offs again. For example, energy spectra cannot be integrated over. One has to apply some minimal energy cut on lower bound, the upper bound is of course given by the experimental possibilities. The same applies to the angular distributions, where boundaries are given by the detector geometry.

At last, it is also important to compare them with the predictions of

Monte-Carlo (MC) simulations. MC simulations are unavoidable in high-energy physics, because they offer comparison between theory and experiment.

4.5 Associated Lepton Production

Jet studies are important for QCD. QCD processes with multijet production are usual background for other processes. Therefore the search for new particles is done via their leptonic final states where the background is not so large. Consider for example the top quark discovered at the Tevatron in 1995. The top quark is created at the Tevatron mostly in pairs with the anti-top quark via the quark-antiquark annihilation (~ 85 %) or gluon-gluon fusion (~ 15 %). It decays before it can hadronize ($t \rightarrow Wb(\sim 100\%)$). The W boson can than decay in several ways. It can decay hadronically into two jets or leptonically into a lepton and its neutrino. Altogether both W's can decay into four jets, to two jets with one lepton and one neutrino or into two leptons and two neutrinos. The b-quarks hadronize and form another two jets. The final state can thus be:

- Alljets channel - six jet in the final state (~ 44 %).
- Single lepton channel - one lepton, one neutrino and four jets (~ 44 %).
- Dilepton channel - two leptons (e or μ) and two neutrinos with two b-quark jets (~ 12 %).

The branching ratios are shown in figure 4.12, showing also different lepton channels.

4.5.1 Lepton Identification

This section will cover only the identification of electrons. Muons are found using muon detectors outside of the calorimeter. The τ lepton identification is more difficult.

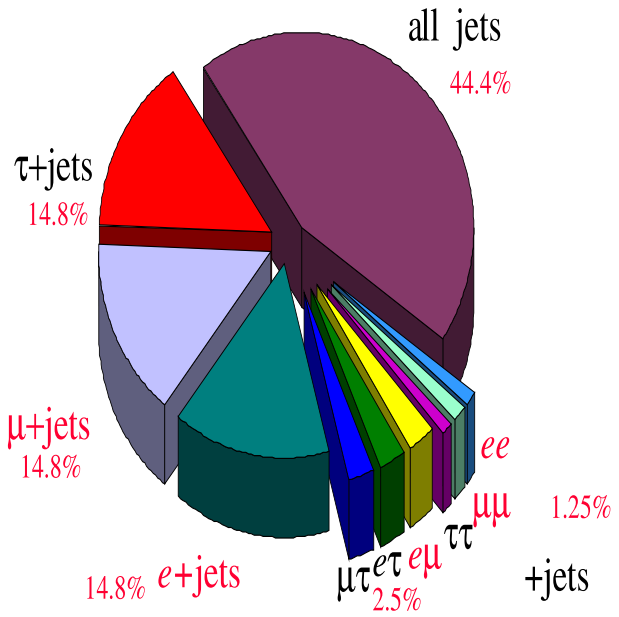

Figure 4.12: Top-antitop quark pair decay channels

Electromagnetical objects are objects with energy deposited mostly in EM layers of the calorimeter. These can be leptons, photons, or jets. EM objects are reconstructed using algorithms which are similar to the algorithms used in the case of jets. Other cuts are used to properly identify electrons from photons or jets.

Following cuts are used in this thesis for electron identification:

- Transverse momentum of an EM object is required to be greater than 15 GeV. Calorimeter can detect a larger number of objects (for example photons or electrons from later decaying particles). The important ones are those ones from initial interaction and will thus carry a large transverse momenta. $p_T > 15\,\mathrm{GeV}$.

- During the reconstruction, objects are assigned different ID values when they pass identification criteria. EM objects passing cluster algorithm will have ID $= 10, \pm 11$.

- EM objects should have most of their energy deposited in the EM layers of the calorimeter. Therefore their EM fraction should be high.

EMF > 0.9. This cut can be set even higher to reduce the number of fake electrons.

- Electrons originating from W and Z boson decays are isolated since these electrons are not produced together with other particles. Isolation variable is used to separate electron from these decays. This electrons are required to have Iso < 0.15.

- From studying properties of showers produced by electrons, a variable measuring of how "electron-like" a shower is computed. It is computed from eight parameters (the four EM layers energy fractions, the total EM energy, vertex z-position and transverse shower width in ϕ and z, which then form a covariance matrix to see how these parameters are correlated. To find how an eventual shape of shower is consistent with an typical electron shower, χ^2 method of the H-matrix is used (H-matrix is the inverse of the covariance matrix). The result is that a cut on HMX8 variable is used HMX8 < 20.

- Electrons can be distinguished from photons by the fact that they have tracks associated with the cluster. Therefore EM object is required to have a track.

The plot 4.13 shows invariant mass distribution in events containing at least two EM objects satisfying the explained criteria. The plot has a peak slightly above 90 GeV, which represents $Z \to e^+e^-$ production. The peak is fitted with double Gaussian, obtaining $M_{Z\to ee} = 91.37\,\text{GeV}$.

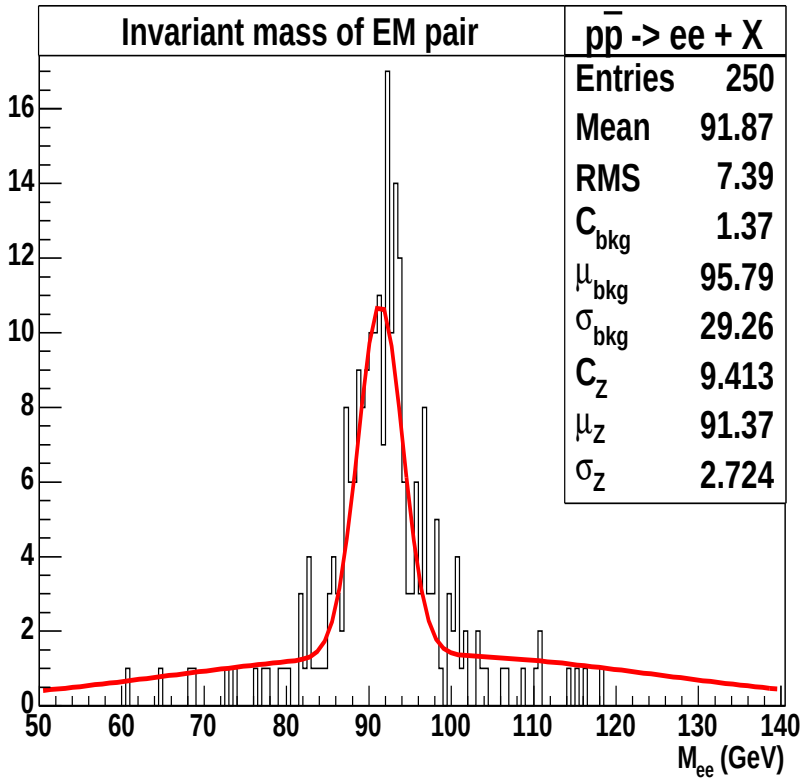

Figure 4.13: Invariant mass of events containing two well defined EM objects, peak is fitted with double Gaussian, obtaining $M_Z = 91.37\,\text{GeV}$.

5 Conclusion

Tevatron is currently the largest hadron collider in the world. Since its upgrade and start of Run II, it is collecting a large statistics of unique data. The analysis of this data will enhance current knowledge about high-energy (or particle) physics. Before the start of the Large Hadron Collider (LHC) at CERN probably in 2008, Tevatron is the only machine, where top quark is produced. Also Higgs boson and some non-Standard Model physics might be discovered there.

Tevatron is performing well just now, the collected luminosity already exceeded the luminosity collected in whole Run I. Data collected between August 2002 and September 2003 is analyzed in this thesis. The work was mainly oriented on the study of jet production and jet energy and angular distribution.

At first some theoretical background of QCD was presented. Then jet definition was described from the experimental point of view. Two main classes of jet algorithms were shown. The class of K_T algorithms have some theoretical advantages compared to cone algorithms, but still is not much used in hadron-hadron collision analysis. For example in Run II at DØ advanced type of cone algorithm is preferred, while K_T is missing Jet Energy Scale correction which prevents comparison of measured quantities to the theoretical predictions.

Next, accelerator complex and detectors were briefly described. The DØ detector's most important part is the calorimeter. In the calorimeter nearly all particles deposite their energies. It is also the part where jets are visible as showers of particles. Other important part of the detector is the inner tracking system, which shows the tracks left by particles and thus enables identification of some of them. The outer part of the detector is the muon sys-

tem which detect the muons that are usually not detected by the calorimeter. Neutrinos as weakly interacting particles are not detected. Their presence is usually deduced from the energy disbalance.

The main chapter was devoted to the jet studies. At first, properties of good jets were defined and described. Corresponding cuts were applied to the available p14 data sample. Properties of all good jets such as transverse energy, transverse momentum and angular distribution were then shown. Finally, inclusive dijet production was studied. In this study only two p_T jets are considered. Again all important distributions were shown. Special part was devoted to the angular distribution. The angular distribution was computed at leading-order of the QCD. Reasonable agreement was found between the data and theory. Further work can improve the results by examining cut efficiencies and luminosity to get cross-section instead of data distribution. Finally, it can be compared with MC prediction.

At last lepton production was discussed. Jet production studies are useful for comparison with QCD, but are very difficult to separate the right signal when decay products of special processes (such as top quark production and others) are investigated. In these cases, lepton final states are easier to study even that the statistics is much lower. Distribution of invariant mass for events containing two well defined electrons was shown with a clear peak fitted at 91.37 GeV corresponding to $q\overline{q} \rightarrow Z \rightarrow e^+e^-$.

Bibliography

[1] Chýla, J., *Quarks, Partons and Quantum Chromodynamics*, www-hep2.fzu.cz/Centrum (2003)

[2] Enberg, R., *Quantum Chromodynamics and Colour Singlet Exchange in High Energy Interactions*, Ph. D. Thesis Summary, http://www3.tsl.uu.se/~enberg/thesis/thesis.pdf

[3] Hinchliffe, I., Manohar, A. V., *The QCD Coupling Constant*, Ann. Rev. Nucl. Part. Sci. **50**, 643 (2000), hep-ph/0004186 v1

[4] Hořejší, J., *Fundamentals of Electroweak Theory*, Karolinum, Praha (2002)

[5] Kolář, K., *Evoluční rovnice kvantové chromodynamiky a jejich řešení*, Diploma Thesis, CU Prague (2003)

[6] Kvita, J., *Effects of Top Quark and W Boson Finite Widths on the Measurement of the Top Quark Mass*, Diploma Thesis, CU Prague (2003)

[7] Owens, J. F., Reya, E., Glück, M., *Detailed quantum-chromodynamics predictions for high-p_T processes*, Phys. Rev. **D18**, 1501 (1978)

[8] Abachi, S., *et al.*, (The DØ Collaboration), *The DØ Detector*, FERMILAB-Pub-93/179-E, 1993, Nucl. Instrum. Meth. **A338**, 185 (1994)

[9] Abachi, S., *et al.*, (The DØ Collaboration), *The DØ Upgrade, The Detector and Its Physics*, FERMILAB-Pub-96/357-E (1996)

[10] Christiansen, T., *Überblick über das DØ-Experiment*, http://www.etp.physik.uni-muenchen.de/d0/d0_de.html

[11] Ellison, J., *The DØ Detector Upgrade and Physics Program*, hep-ex/0101048, v2 (2001)

[12] Křivková, P., *Report of diffractive scattering at D0*, http://www-d0.fnal.gov/ krivkova/report.html (2001)

[13] Lipton, R., *D0 Run IIa Trigger Commissioning*, http://d0server1.fnal.gov/users/lipton/www/Trigger.html

[14] Malamud, E., *Fermilab's Chain of Accelerators, Accelerator Details*, http://www-ad.fnal.giv/public/chain.html (2000)

[15] Protopopescu, S., Denisov D., Linnemann, J., *Coordinate Systems And Units For D0 Software*, http://www-d0online.fnal.gov/www/groups/cap/quick_guide/Coordinate_System.htm (2002)

[16] *The D0 Upgrade*, http://www-d0.fnal.gov/hardware/upgrade/pac0495/d0upgr.html (1995)

[17] Blazey, G. C., *et. al.*, *Run II Jet Physics*, hep-ex/0005012, v2 (2000)

[18] Catani, S., Dokshitzer, Yu. L., *The $k_\perp$-Clustering Algorithm for Jets in Deep Inelastic Scattering and Hadron Collisions*, CERN-TH.6473/92 (1992)

[19] Chekanov, S. V., *Jet algorithms: a minireview*, hep-ph/0211298 (2002)

[20] Duflot, L., Grivaz, J.-F., Ridel, M., Verdier, P., *Jets in high E_T events: data vs. Monte Carlo*, DØ Note 4020 (2002)

[21] Glover, N., *Jets at Hadron Colliders*, CTEQ 2001 Summer School Lecture, http://www.phys.psu.edu/ cteq/schools/summer01/jets/ (2001)

[22] Hubáček, Z., *Studium multijetových koncových stavů*, Research work CTU FNSPE (2003), (in czech)

[23] Hubáček, Z., *Rešerše strukturních funkcí protonu, Určování konstanty α_S silných interakcí z produkcí mnoha jetů*, Review work CTU FNSPE (2002), (in czech)

[24] Juránek, V., *Jety jako nástroj studia struktury hmoty*, Research work CTU FNSPE (2002), (in czech)

[25] Kupčo, A., Begel, M., Demine, P., Royon, Ch., Wobisch, M., Zieliński, M., *Measurement of dijet azimuthal angle distribution in $p\overline{p}$ collisions at $\sqrt{s} = 1.96$TeV*, DØ Note 4384 (2004)

[26] Kupčo, A., *Measurement and QCD analysis of inclusive dijet mass cross section in $p\bar{p}$ collisions at $\sqrt{s} = 1.96$ TeV*, Doctoral Thesis, CU Prague (2003)

[27] Kupčo, A., Demine, P., Royon, Ch., Zieliński, M., *Measurement of the dijet mass cross section*, DØ Note 4145 (2003)

[28] Kupčo, A., *JetID certification for p14 data*, http://www-d0.fnal.gov/~kupco/d0_private/jetID_p14.html (2003)

[29] Kupčo, A., *Měření inclusivního účinného průřezu invariantní hmoty dijetu v DØ Run II datech*, http://www-hep2.fzu.cz/~kupco/phd/talks/fzu-20030310.ps.gz (2003)

[30] Steinbrück, G., *Measurement of the Angular Distribution of Electrons from W Boson Decays at DØ*, PhD. Dissertation, University of Oklahoma (1999)

[31] Varelas, N., *Jet Physics Lecture II*, CTEQ Summer School 2001 Lecture, http://www.phys.psu.edu/ cteq/schools/summer01/jets/ (2001)

[32] Kupčo, Alexander, DAPNIA-Saclay, private communication

[33] Kvita, Jiří, Charles University, Prague, private communication

[34] Otec, Roman, Czech Technical University in Prague, Prague , private communication

[35] Soustružník, Karel, Charles University, Prague, private communication

[36] Melanson, H., *How To Run Reco*, http://www-d0.fnal.gov/computing/algorithms/howto/howtoreco.html (2002)

[37] Schildt, H., *C++ from the Ground Up*, Third Edition, McGraw-Hill/Osborne (2003)

[38] *ROOT - An Object-Oriented Data Analysis Framework*, http://root.cern.ch